Received: 19 December 2021 | Revised: 2 August 2022 | Accepted: 7 August 2022

DOI: 10.1002/hbm.26129

RESEARCH ARTICLE

WILEY

The complexity of spontaneous brain activity changes in schizophrenia, bipolar disorder, and ADHD was examined using different variations of entropy

Sihai Guan[1] | Dongyu Wan[2] | Rong Zhao[2] | Edgar Canario[3] | Chun Meng[2] | Bharat B. Biswal[2,3]

[1]Key Laboratory of Electronic and Information Engineering, State Ethnic Affairs Commission, College of Electronic and Information, Southwest Minzu University, Chengdu, China

[2]The Clinical Hospital of Chengdu Brain Science Institute, MOE Key Laboratory for Neuroinformation, Center for Information in Medicine, School of Life Science and Technology, University of Electronic Science and Technology of China, Chengdu, China

[3]Department of Biomedical Engineering, New Jersey Institute of Technology, Newark, New Jersey, USA

Correspondence
Bharat B. Biswal, Department of Biomedical Engineering, New Jersey Institute of Technology, 607 Fenster Hall, University Height, Newark, NJ 07102, USA.
Email: bbiswal@yahoo.com

Chun Meng, The Clinical Hospital of Chengdu Brain Science Institute, MOE Key Laboratory for Neuroinformation, Center for Information in Medicine, School of Life Science and Technology, University of Electronic Science and Technology of China, No. 2006, Xiyuan Avenue, Chengdu 611731, China.
Email: chunmeng@uestc.edu.cn

Abstract

Adult attention deficit/hyperactivity disorder (ADHD), schizophrenia (SCHZ), and bipolar disorder (BP) have common symptoms and differences, and the underlying neural mechanisms are still unclear. This article will thoroughly discuss the differences between ADHD, BP, and SCHZ (31 healthy control and 31 ADHD; 34 healthy control and 34 BP; 42 healthy control and 42 SCHZ) relative to healthy subjects in combination with three atlases (et al., the Brainnetome atlas, the Dosenbach atlas, the Power atlas) and seven entropies (et al., approximate entropy (ApEn), sample entropy (SaEn), permutation entropy (PeEn), fuzzy entropy (FuEn), differential entropy (DiffEn), range entropy (RaEn), and dispersion entropy (DispEn)), as well as the prominent significant brain regions, in the hope of giving information that is more suitable for analyzing different diseases' entropy. First, the reliability (et al., intraclass correlation coefficient [ICC]) of seven kinds of entropy is calculated and analyzed by using the MSC dataset (10 subjects and 100 sessions in total) and simulation data; then, seven types of entropy and multiscale entropy expanded based on seven kinds of entropy are used to explore the differences and brain regions of ADHD, BP, and SCHZ relative to healthy subjects; and finally, by verifying the classification performance of the seven information entropies on ADHD, BP, and SCHZ, the effectiveness of the seven entropy methods is evaluated through these three methods. The core brain regions that affect the classification are given, and DiffEn performed best on ADHD, SaEn for BP, and RaEn for SCHZ.

KEYWORDS
(multiscale)entropies, ADHD/BP/SCHZ, different atlases, resting-state fMRI, test–retest reliability

1 | INTRODUCTION

The human brain is a complex system characterized by large-scale distributed neural networks of inherently fluctuating signals, revealed by accumulating functional magnetic resonance imaging (fMRI) studies (Biswal et al., 2010; Deco et al., 2011; Gordon et al., 2017). Resting-state fMRI (rs-fMRI) can reflect the spontaneous neural activity of the human brain and can be used to study its intrinsic function. In the past

decades, resting-state functional connectivity (rsFC) has been increasingly used in mapping the intrinsic functional networks of the human brain, with a focus on the inherently fluctuating signals and their interactions between different brain regions (Biswal et al., 1995; Fox & Greicius, 2010; Greicius et al., 2003, 2009). There are numerous complexity methods of rs-fMRI brain signals, such as the Lyapunov exponent, correlation dimension, Lempel-Ziv complexity, Hurst exponent, and entropy (Ali et al., 2018; Guan et al., 2020, 2022; Ju et al., 2019; Lin et al., 2022; Smith et al., 2013; Yakovleva et al., 2020). Among these methods, due to its simple algorithm, the small amount of data required, and the strong anti-noise ability in calculation, entropy is one of the most widely used complexity methods for evaluating the dynamic characteristics of brain signals. In physiological signal analysis, entropy methods have been widely used, including approximate entropy (ApEn; Yentes et al., 2012), sample entropy (SaEn; Richman et al., 2004), fuzzy entropy (FuEn; Chen et al., 2007), and permutation entropy (PeEn; Bandt & Pompe, 2002). SaEn, as proposed by Richman and Moorman (2000), is an improved version of Pincus's ApEn and aims to overcome the limitations of ApEn and reduce statistical bias. FuEn is an improvement over the ApEn and SaEn algorithms. PeEn, another widely used entropy measure, is a novel method developed by Bandt to characterize the complexity of time series (Bandt & Pompe, 2002). PeEn is suitable for capturing the complex dynamics and rich time structure embedded in biological systems.

Besides, there are some scholars have also proposed new entropy methods, such as Range entropy (RaEn; Omidvarnia et al., 2018), Dispersion entropy (DispEn; Rostaghi & Azami, 2016), and Differential entropy (DiffEn; Duan et al., 2013). RaEn is a proposed modification to ApEn and SaEn, which are highly sensitive to signal amplitude changes and less affected by variation in the magnitude of signals. DispEn originates from SaEn and PeEn, which can detect the noise bandwidth and simultaneous frequency and amplitude change. It does not lead to undefined results in short signals, is less sensitive to noise, and is considerably faster than SaEn. DiffEn is used to measure the complexity of a continuous random variable, is the entropy of a continuous random variable, and is also related to minimum description length. However, relatively few studies have employed these entropies simultaneously approach for fMRI (Lin et al., 2019; Sokunbi et al., 2011, 2013, 2014, 2015). Specifically, Sokunbi et al. (2011) conducted multiple fMRI signal studies using different entropy measures. Using ApEn to study individual differences in cognitive performance in an elderly population, the results showed that higher regional signal entropy was associated with better cognitive performance. SaEn was used to study the complexity of fMRI signals in the brain of schizophrenia (SCHZ) patients. It was found that the complexity of the signals from these patients was higher than that of HC at the global and local levels (Sokunbi et al., 2014). They also used SaEn to analyze the patients' fMRI signals from attention-deficit/hyperactivity disorder (ADHD). They found that the entropy values of the fMRI signal from the whole brain of these patients were lower than those of the controls (Sokunbi et al., 2013). The analysis of the complexity of fMRI signals from 41 HC adults (41 males, 19–85 years old) showed that brain entropy (BEN) values at the global and local levels were negatively correlated with age (Sokunbi et al., 2015). Lin et al. (2019) used SaEn to explore changes in the entropy of fMRI signals from the brains of patients with depression. Compared with HC, patients with depression showed reduced entropy in the medial orbitofrontal cortex and cingulate cortex but increased brain signal complexity in the motor cortex. These studies showed that entropy measures could analyze the temporal changes in fMRI signals and locate the relevant brain space. Studies on fMRI showed that the change in entropy value can act as a biomarker for disease states and can also be used to study the internal mechanism of the HC human brain.

Furthermore, a few studies have systematically analyzed the test–retest reliability of these entropy methods applied to fMRI signals to determine the entropy method that most reliably reflects the complexity of biological systems (Liu et al., 2020; Niu et al., 2020). For example, Niu and colleagues (Niu et al., 2020) investigated the distribution and test–retest reliability of four entropy measures in three independent data sets. They showed that analyzing fMRI signals with entropy showed strong tissue sensitivity, with PeEn and FuEn superior to ApEn and SaEn at all three levels. ApEn and SaEn are two of the most commonly used measures in contemporary science among the signal mentioned above entropy measures. SaEn stems from ApEn after addressing some limitations, including inconsistency and strong dependency on the input signal length. However, both measures still suffer from sensitivity to signal amplitude changes. Although PeEn is conceptually simple and computationally fast, the method does not consider the mean value of amplitudes and the differences between amplitude values (Rostaghi & Azami, 2016). Liu et al. (2020) examined the Human Connectome Project data (https://www.humanconnectome.org and have been described extensively in the literature; Van Essen et al., 2013) of 998 healthy young adults (age range: 22–35 years). They demonstrated the crucial influence of test–retest reliability on detecting individual differences in entropy-based studies with fingerprint identification (Finn et al., 2015) applied to whole-cortex entropy profiles. In addition, Zhang and colleagues (Zhang et al., 2021) used multiscale sample entropy of rs-fMRI from 15 SCHZ, 49 BP, and 49 HC to assess differences in rs-fMRI signal complexity. Niu et al. (2020) compared the test–retest reliability of ApEn, SaEn, FuEn, and PeEn, results showed that the highest test–retest reliability was achieved with PeEn and FuEn were superior to ApEn and SaEn at all three levels, that is, based on voxels, brain regions, and functional networks. However, brain rs-fMRI signals are very susceptible to noise during the acquisition process, so anti-noise performance of entropy is important (Niu et al., 2019). DiffEn, DispEn, and RaEn are not currently used in rs-fMRI, so whether DiffEn, DispEn, and RaEn are likely to have better anti-noise performance is a new topic that warrants exploration.

Based on three different atlases, this article will focus on finding a reliable and effective entropy method to reveal differences in functional connectivity between ADHD, BP, and SCHZ. So, the distribution and test–retest performance of the seven entropy methods (ApEn, SaEn, PeEn, FuEn, DiffEn, DispEn, and RaEn) in this aim were also compared. The similarities and differences between ADHD, BP, and SCHZ as revealed by entropy methods, are also explored.

Additionally, multiscale entropy expanded based on the seven kinds of entropy is used to analyze the differences and brain regions of ADHD, BP, and SCHZ relative to healthy subjects. The entropy methods that are most effective in these tasks will be determined using classification analysis.

2 | MATERIALS AND METHODS

2.1 | Resting-state fMRI data

The MSC datasets used in this study were obtained from the OpenfMRI's data repository (https://openfmri.org) with the project name "The Midnight Scan Club (MSC) dataset." It consists of 10 healthy, right-handed, young adult subjects (5 females; age: 24–34; Gordon et al., 2017). The MRI data were acquired on a Siemens TRIO 3T MRI scanner. The imaging was conducted on 10 subsequent days, each beginning at midnight. A summary only is provided because details of the MSC study have been provided in previous literature (Gordon et al., 2017) and online (https://openneuro.org/datasets/ds000224) here. The rs-fMRI data was collected using a gradient-echo planar image (EPI) sequence (TR = 2.2 s, TE = 27 ms, flip angle = 90°, 36 slices, and 4 mm isotropic voxels). Within each session of 10 subsequent days, 30 min of rs-fMRI data were collected, in which subjects visually fixated on a white crosshair presented against a black background. One subject (MSC08) was excluded due to falling asleep during the scan, in line with previous literature (Gordon et al., 2017). Therefore, the rs-fMRI data of 9 subjects with 10 sessions were analyzed in this study.

The Consortium for Neuropsychiatric Phenomics dataset used in this study was obtained from the OpenfMRI database with the accession number ds000030 (https://www.openfmri.org/dataset/ds000030/). All participants gave written informed consent during the UCLA Consortium for Neuropsychiatric Phenomics (CNP) LA5c Study data collection. The CNP published a dataset (Poldrack et al., 2016) with neuroimaging and phenotypic information for 272 participants. The subject population consists of HC (130 subjects), as well as participants with diagnoses of adult ADHD (43 subjects), BP (49 subjects), and SCHZ (50 subjects). The sample of subjects contains 155 men and 117 women, with ages between 21 and 50 years (mean: 33.23; median: 31.0). Each subject completed at least 8 years of formal education and have either English or Spanish as a primary language. Subjects were recruited by community advertisement and outreach to local clinics and online portals. The consortium excluded patients with diagnoses in at least two different patient groups. Furthermore, the following exclusion criteria were used: left-handedness, pregnancy, history of head injury with loss of consciousness, or other contraindications to scanning. Neuroimaging data were acquired on a 3T Siemens Trio scanner. Functional MRI data were collected with a T2*-weighted EPI sequence with slice thickness = 4 mm, 34 slices, TR = 2 s, TE = 30 ms, flip angle = 90°, matrix = 64 × 64, FOV = 192 mm. A T1-weighted high-resolution anatomical scan was collected with the following parameter: slice thickness = 1 mm, 176 slices, TR = 1.9 s, TE = 2.26 ms, matrix = 256 × 256, FOV = 250 mm.

In the current study, we included healthy subjects and subjects with ADHD, BP, and SCHZ. We removed those with large head motions for subjects with ADHD, BP, SCHZ, and HC. In addition, the age and gender of each disease group and the corresponding control group are required to be similar. Then, framewise displacement was calculated, and subjects were excluded if their maximum translation or rotation framewise displacement was greater than 2 mm. We then manually chose age and gender-matched HC subjects. As a result, 31 HC and 31 ADHD; 34 HC and 34 BP; 42 HC and 42 SCHZ remained for the current study.

2.2 | Data preprocessing

For each subject and each session, those two rs-fMRI datasets were preprocessed by using SPM12 (Ashburner, 2012) and DPABI (Yan et al., 2016), with the following steps: (1) discarding the first 10 volumes for the equilibrium of magnetization; (2) slice timing correction to account for temporal shifts during data acquisition; (3) motion contaminated volumes were then identified by frame-by-frame displacement [FD, described in Power et al. (2011)], calculated as the sum of absolute values of the differentials of the three translational motion parameters (including one filtered parameter) and three rotational motion parameters. Frames with FD >0.2 mm were flagged as motion-contaminated; (4) regressing out nuisance variables including the Friston-24 head motion time-series (Friston et al., 1996) as well as the average time-series of white matter, cerebrospinal fluid, and global signal (Fox & Raichle, 2007); (5) normalizing functional images into the standard Montreal Neurological Institute space by using the EPI atlas with the resampled voxel size of 3 mm; (6) smoothing by using a 6mm full width at half maximum (FWHM) Gaussian kernel; (7) band-pass filtering (0.009–0.08 Hz); and (8) Scrubbing settings: FD type refer Power, FD threshold for bad time is 0.2 mm, and scrubbing time points before and after bad time is one and two, respectively. The scrubbing method was a linear interpolation, and Linear interpolation refers to a method that uses a straight line connecting two known quantities to determine an unknown value between the two known quantities. The interpolation function in MATLAB2016b is "interp1.m." The analytical pipeline is illustrated in Figure 1.

2.3 | Entropy calculation

To compare the test–retest reliability of entropy methods, we applied entropy to investigate the complexity of rs-fMRI signals. Entropy is the rate of new information generation, which measures the probability of generating a new pattern in the signal. The greater the probability of generating a new pattern, the greater the signal complexity. This value was calculated with the following formula:

$$H = -\sum_{i=1}^{n} p_i \log p_i \quad (1)$$

In the formula, p_i represents the probability of the i-th discrete state.

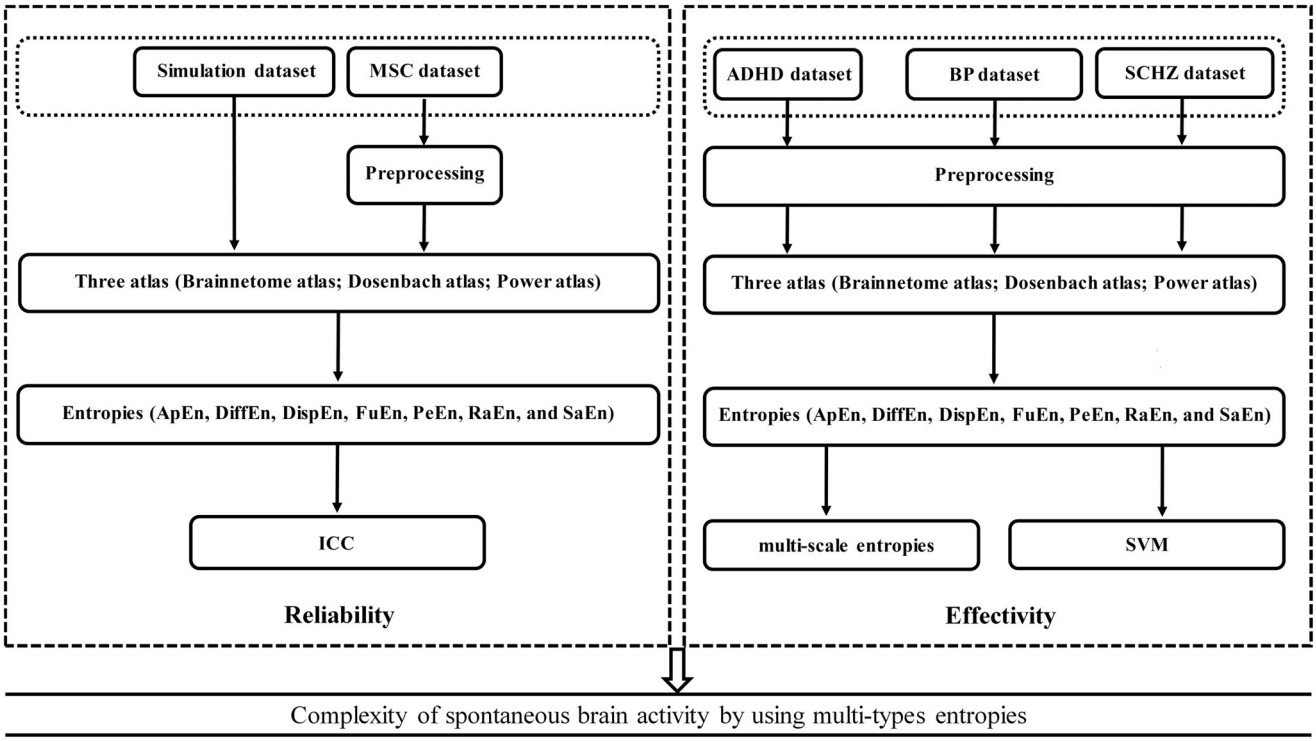

FIGURE 1 The flowchart of the complexity of spontaneous brain activity by using multi-type entropies. The raw rs-fMRI images of the MSC dataset and UCLA dataset underwent preprocessing and time-series extraction and then were used to compute entropy values using seven entropy methods. The entropy analysis was conducted based on whole-brain gray matter voxels. Test–retest reliability was finally examined using the intraclass correlation coefficient (ICC). Besides, altered complexity of spontaneous brain activity and classification results were explored

Here, seven entropy methods were applied as complexity estimators of rs-fMRI signals:

2.3.1 | Approximate entropy

ApEn (Sokunbi et al., 2015) is roughly equivalent to the mean value of the logarithmic conditional probability of the new state appearing when the dimension changes. It has a certain value in measuring the complexity of the time-series. Its calculation formula can be expressed as follows.

Step 1: Given a time series with N data points $\{x(1), x(2), \cdots, x(N)\}$, and a priori determination of two unknown parameters, m and r. The parameter m determines the length of the sequences to be compared, and its selection can be estimated by calculating the false nearest neighbor. The second parameter, r, is the tolerance threshold for accepting similar patterns between two segments and has been recommended to be within 0.1–0.2 times the standard deviation of the data.

Step 2: By reconstructing the original data, subsequences can be obtained with $N-m+1$ data points $\{X(1), X(2), \ldots, X(N-m+1)\}$, where $X(i)=\{x(1), x(2), \ldots, x(i+m-1)\}$.

Step 3: Calculate the distance $d_m=[X(i), X(j)]$, the distance d_m is determined by the maximum difference between the corresponding position elements in the two vectors. This includes the distance $i=j$.

Step 4: Then count the number of vectors that satisfy the following conditions, and find the ratio between them and the total number of statistics:

$$C_i^m(r)=\frac{\text{num}[d_m=[X(i),\ X(j)]<r]}{N-m+1} \tag{2}$$

This process is called the atlas matching process of $X(i)$, $C_i^m(r)$ represents the probability of matching between any $X(j)$ and the atlas.

Step 5: Define the average similarity rate when the number of subsequences is m:

$$\Phi_m(r)=\frac{\sum_{i=1}^{N-m+1}\log\left[C_i^m(r)\right]}{N-m+1} \tag{3}$$

Step 6: According to the above 1–5, calculate the average similarity rate $\Phi_{m+1}(r)$ when the number of divided subsequences is $m+1$.

Step 7: Get approximate entropy:

$$ApEn=\Phi_m(r)-\Phi_{m+1}(r). \tag{4}$$

2.3.2 | Sample entropy

SaEn (Richman & Moorman, 2000) is an improvement relative to the ApEn algorithm in that SaEn calculates the logarithm of the sum and aims to reduce the ApEn's error to is more closely consistent with the known random part. Its calculation formula can be expressed as follows.

Step 1: Given a time series with N data points $\{x(1), x(2), ..., x(N)\}$, and a priori determination of two unknown parameters, m and r. The parameter m determines the length of the sequences to be compared, and its selection can be estimated by calculating the false nearest neighbor. The second parameter, r, is the tolerance threshold for accepting similar patterns between two segments and has been recommended to be within 0.1–0.2 times the standard deviation of the data.

Step 2: By reconstructing the original data, subsequences can be obtained with $N-m+1$ data points $\{X(1), X(2), ..., X(N-m+1)\}$, where $X(i)=\{x(1), x(2), ..., x(i+m-1)\}$.

Step 3: Calculate the distance $d_m=[X(i), X(j)]$, the distance d_m is determined by the maximum difference between the corresponding position elements in the two vectors. This includes the distance $i \neq j$.

Step 4: Then count the number of vectors that satisfy the following conditions, and find the ratio between them and the total number of statistics:

$$B_i^m(r)=\frac{\text{num}[d_m=[X(i),\ X(j)]<r]}{N-m} \tag{5}$$

This process is called the atlas matching process of $X(i)$, $B_i^m(r)$ represents the probability of matching between any $X(j)$ and the atlas.

Step 5: Define the average similarity rate when the number of subsequences is m:

$$\Phi_m(r)=\frac{\sum_{i=1}^{N-m+1}\log\left[B_i^m(r)\right]}{N-m+1} \tag{6}$$

Step 6: According to the above 1–5, calculate the average similarity rate $\Phi_{m+1}(r)$ when the number of divided subsequences is $m+1$.

Step 7: Get approximate entropy:

$$SaEn=-\ln\frac{\Phi_{m+1}(r)}{\Phi_m(r)}. \tag{7}$$

2.3.3 | Fuzzy entropy

FuEn (Chen et al., 2007) adds a fuzzy function to the comparison of continuous point vectors and generalizes these vectors to reduce the impact of measurement drift. Its calculation formula can be expressed as follows.

Step 1: Given a time series with N data points $\{x(1), x(2), ..., x(N)\}$, and a priori determination of two unknown parameters, m and r. The parameter m determines the length of the sequences to be compared, and its selection can be estimated by calculating the false nearest neighbor. The second parameter, r, is the tolerance threshold for accepting similar patterns between two segments and has been recommended to be within 0.1–0.2 times the standard deviation of the data.

Step 2: By reconstructing the original data, subsequences can be obtained with $N-m+1$ data points $\{X(1), X(2), ..., X(N-m+1)\}$, where $X(i)=\{x(1), x(2), ..., x(i+m-1)\}-\frac{1}{m}\sum_{k=1}^{m-1}x(i+k)$.

Step 3. Calculate the distance $d_m=[X(i), X(j)]$, the distance d_m is determined by the maximum difference between the corresponding position elements in the two vectors. This includes the distance $i \neq j$.

Step 4: The fuzzy membership function:

$$A_{ik}^m(r)=\exp\left[-\left(\frac{d_{ik}^m(r)}{r}\right)^n\right] \tag{8}$$

This process is called the atlas matching process of $X(i)$, $B_i^m(r)$ represents the probability of matching between any $X(j)$ and the atlas.

Step 5: Define the average similarity rate when the number of subsequences is m:

$$\Phi_i^m(r)=\frac{\sum_{j=1,i\neq j}^{N-m+1}A_{ik}^m(r)}{N-m} \tag{9}$$

Step 6: According to the above 1–5, calculate the average similarity rate $\Phi_{m+1}(r)$ when the number of divided subsequences is $m+1$.

Step 7: Get fuzzy entropy:

$$FuEn=\ln\Phi_{m+1}(r)-\ln\Phi_m(r). \tag{10}$$

2.3.4 | Permutation entropy

PeEn (Bandt & Pompe, 2002) uses the shape of neighboring points to evaluate complexity based on permutation patterns, and it has good computing performance for analyses of any real-world data. Its calculation formula can be expressed as follows.

Step 1: Given a time series with N data points $\{x(1), x(2), ..., x(N)\}$, and a priori determination of two unknown parameters, m and L. The parameter m determines the length of the sequences to be compared, and its selection can be estimated by calculating the false nearest neighbor. The second parameter, L, is the delay time.

Step 2: By reconstructing the original data, subsequences can be obtained with $N-m+1$ data points $\{X(1), X(2), ..., X(N-m+1)\}$, where $X(i)=\{x(1), x(L), ..., x((m-1)L)\}$.

Step 3: Then do an increasing sort internally for each $X(i)$, that is $x(i+(j_1-1)L)\leq x(i+(j_2-1)L)\leq\cdots\leq x(i+(j_m-1)L)$. If two values are equal, sort them according to the subscript i of j_i. In this case, an $X(i)$ is mapped to, which is exactly one of $m!$ permutations. That is, every m dimensional subsequence $X(i)$ is mapped to one of $m!$ permutations.

Step 4: Through the above Step 1–Step 3, the continuous m dimensional subspace is represented by such a sequence of symbols, where the number of these symbols is $m!$. Denote the probability distribution of all symbols in terms of P_1,P_2,...,P_K, where $K\leq m!$.

Step 5: Get permutation entropy:

$$PeEn = -\sum_{j=1}^{K} P_j \ln P_j. \quad (11)$$

2.3.5 | Dispersion entropy

DispEn is calculated by first conducting permutations based on the original time series (Rostaghi & Azami, 2016). DispEn can detect the noise bandwidth and simultaneous frequency and amplitude change. Also, it originates from SaEn and PeEn. Its calculation formula can be expressed as follows.

Step 1: Given a time series with N data points $\{x(1), x(2), ..., x(N)\}$, and a priori determination of two unknown parameters, m and c. The parameter m determines the length of the sequences to be compared, and its selection can be estimated by calculating the false nearest neighbor. The second parameter, c, is the number of classes that can be members of the time series. We first employ the normal cumulative distribution function to map $\{x(1), x(2), ..., x(N)\}$ into $\{y(1), y(2), ..., y(N)\}$ from 0 to 1. and a priori determination of two unknown parameters, m and L. The parameter m determines the length of the sequences to be compared, and its selection can be estimated by calculating the false nearest neighbor. The second parameter, L, is the delay time.

Step 2: We use a linear algorithm to assign each $y(k)$ to an integer from 1 to c. To do so, for each member of the mapped signal, we use $z_k^c = \text{round}(cy(k) + 0.5)$, where z_k^c shows the kth member of the classified time series and rounding involves increasing or decreasing a number to the next digit.

Step 3: Each embedding vector $z_k^{m,c}$ with embedding dimension m and time delay L is created according to $z_k^{m,c} = \left\{z_k^c, z_{k+L}^c, ..., z_{k+(m-1)L}^c\right\}, k = 1,2,...,N-(m-1)L$. Each time series $z_k^{m,c}$ is mapped to a dispersion pattern $\rho_{v0v1...vm-1}$, where $z_k^c = v0$, $z_{k+L}^c = v1,...,z_{k+(m-1)L}^c = vm-1$. The number of possible dispersion patterns that can be assigned to each time series $z_k^{m,c}$ is equal to c^m, since the signal has m members and each member can be one of the integers from 1 to c.

Step 4: For each of c^m potential dispersion patterns, relative frequency is obtained as follows:

$$p(\rho_{v0v1...vm-1}) = \frac{\text{num}\left[k | k \le N-(m-1)L, z_k^{m,c} hasytpe \rho_{v0v1...vm-1}\right]}{N-(m-1)L} \quad (12)$$

Step 5: Get dispersion entropy:

$$DispEn = -\sum_{\pi=1}^{c^m} p(\rho_{v0v1...vm-1}) \ln p(\rho_{v0v1...vm-1}) \quad (13)$$

2.3.6 | Differential entropy

DiffEn is equivalent to the logarithm energy spectrum in a specific frequency band and was employed to construct features in the frequency bands mentioned above (Duan et al., 2013). Its calculation formula can be expressed as

$$p(X) = -\int_X f(x) \log(f(x)) dx, \quad (14)$$

where X is a random variable, $f(x)$ is the probability density function of X. For the time series X obeying the Gauss distribution $N(0, \sigma^2)$, its DiffEncan be defined as,

$$DiffEn = -\int_{-\infty}^{\infty} \frac{1}{\sqrt{2\pi\sigma^2}} \exp\left(-\frac{x^2}{2\sigma^2}\right) \log\left(\frac{1}{\sqrt{2\pi\sigma^2}} \exp\left(-\frac{x^2}{2\sigma^2}\right)\right) dx = \frac{1}{2}\log\left(2\pi e\sigma^2\right) \quad (15)$$

where σ^2 denotes the DiffEnof the corresponding rs-fMRI signal variance.

2.3.7 | Range entropy

RaEn is a proposed modification to ApEn and SaEn, and the idea here is to estimate the (logarithmic) likelihood that runs of patterns that are close remain close following incremental comparisons (Omidvarnia et al., 2018). Its calculation formula can be expressed as follows.

Step 1: Given a time series with N data points $\{x(1), x(2), ..., x(N)\}$, and a priori determination of two unknown parameters, m and r. The parameter m determines the length of the sequences to be compared, and its selection can be estimated by calculating the false nearest neighbor. The second parameter, r, is the tolerance threshold for accepting similar patterns between two segments and has been recommended to be within 0.1–0.2 times the standard deviation of the data.

Step 2: By reconstructing the original data, subsequences can be obtained with $N-m+1$ data points $\{X(1), X(2), ..., X(N-m+1)\}$, where $X(i) = \{x(1), x(2), ..., x(i+m-1)\}$.

Step 3: Calculate the distance $d_m = [X(i), X(j)]$, as follows

$$d_m = \frac{max_k|X(i+k)-X(j+k)| - min_k|X(i+k)-X(j+k)|}{max_k|X(i+k)-X(j+k)| + min_k|X(i+k)-X(j+k)|}, k = 0,1,...,m-1 \quad (16)$$

In the spacial case of two-dimensional reconstructed phase space ($m = 2$), $d_m = \frac{\max((x(i)-x(j)),\ (x(i+1)-x(j+1))) - \min((x(i)-x(j)),\ (x(i+1)-x(j+1)))}{\max((x(i)-x(j)),\ (x(i+1)-x(j+1))) + \min((x(i)-x(j)),\ (x(i+1)-x(j+1)))}$.

Step 4. Then count the number of vectors that satisfy the following conditions, and find the ratio between them and the total number of statistics:

$$B_i^m(r) = \frac{\text{num}[d_m = [X(i),\ X(j)] < r]}{N-m} \quad (17)$$

This process is called the atlas matching process of $X(i)$, $B_i^m(r)$ represents the probability of matching between any $X(j)$ and the atlas.

Step 5: Define the average similarity rate when the number of subsequences is m:

$$\Phi_m(r) = \frac{\sum_{i=1}^{N-m+1} \log\left[B_i^m(r)\right]}{N-m+1} \tag{18}$$

Step 6: According to the above 1–5, calculate the average similarity rate $\Phi_{m+1}(r)$ when the number of divided subsequences is $m+1$.

Step 7: Get approximate entropy:

$$RaEn = -\ln\frac{\Phi_{m+1}(r)}{\Phi_m(r)}. \tag{19}$$

2.4 | Parameter selection

This study uses three fMRI datasets to compare the test–retest performance of the seven entropy methods. ApEn, SaEn, RaEn, and FuEn need to set three parameters: N, m, and r. N is the number of time points, m specifies the dimension of the phase space, and r is the similarity tolerance. Many studies have discussed the setting of these parameters (Schultz et al., 2008; Tocado et al., 2009). The parameter m is taken as 2, and the similarity tolerance r is taken as 0.25 times the standard deviation of the original data. The PeEn algorithm also involves the setting of three parameters: N, pm, and τ, where N is the time-series, pm is the embedding dimension, and τ is the delay time. The pm value setting is based on the following considerations: when $pm < 3$, the process is meaningless because there are too few permutations and combinations; the larger the pm is, the more the algorithm time complexity will increase as larger m corresponds to more permutations. Bandt and Pompe suggested that pm should be 3–7 (Bandt & Pompe, 2002); Li et al. (2014), to ensure sensitivity to the transient characteristics of the system, suggested that the pm should be a small value to reduce the time complexity of the algorithm. In this study, pm was set as 4. For the time delay in the sorting and symbolization process, the value used in this study was 1. In this setting, more information can be captured in brain signals. The DispEn involves the setting of 4 parameters: pm, nc, ma, and τ, where pm is the embedding dimension, τ is the delay time, nc is the number of classes which usually equal to a number between 3 and 9, and ma is the mapping approach, chosen from "LM" (linear mapping), "NCDF" (normal cumulative distribution function), "TANSIG" (tangent sigmoid), "LOGSIG" (logarithm sigmoid), and "SORT" (sorting method; Azami & Escudero, 2018). There are fewer number parameters in DiffEn: range, and level, where the range is assumed to be a rectangle and the level is the depth in the tree with a default is 0.

2.5 | Multiscale entropy calculations

The multiscale entropy analysis was introduced to estimate the entropy on multiple time scales. The multiscale entropy calculation can be summarized as follows.

Step 1: a coarse-grained time series according to a range of scale factors was constructed;

Step 2: the entropy of each coarse-grained time series was quantified;

Step 3: the multiscale entropy profile was examined using a range of scales.

The length of each coarse-grained time series was equal to the length of the original time series divided by the scale factor. For scale 1, the time series was simply the original time series. So, in this article, all seven entropy methods mentioned in this article are extended to multi-scale entropy, and the results of those seven multi-scale entropies are further analyzed.

2.6 | Test–retest reliability

The test–retest reliability evaluates the statistical stability of the index at different measurement times (Spitzer, 1992). It comprehensively considers the changes within the individual and among different individuals, reflecting the stability and consistency of the index across time (Rongsawad et al., 2019). Test–retest reliability is essential in various fields, including sociology, behavior, physics, biology, and medicine (Chambers, 1985). Due to the interference of various factors in the actual measurement, it is critical to choose a reliable index. The intraclass correlation coefficient (ICC) is a commonly used reliability coefficient index to measure test–retest reliability (Spitzer, 1992). The ICC of intrinsic functional networks was computed as shown below.

$$\mathrm{ICC} = \frac{\mathrm{BMS} - \mathrm{EMS}}{\mathrm{BMS} + (m-1)\mathrm{EMS}} \tag{20}$$

Equation (20) estimates the correlation of the subject signal intensities between sessions, modeled by a two-way ANOVA, with random subject effects and fixed session effects (Shrout & Fleiss, 1979). The BMS is the between-subject mean square, the EMS is the within-subject error mean square, and m is the number of repeated sessions. Furthermore, the ICC values of brain entropies (BENs) were compared with and without band-pass filtering to evaluate the influence of filtering on the test–retest reliability of entropy values. In this study, ICC values were usually divided into five common intervals: $0 < \mathrm{ICC} \le 0.25$ indicated poor reliability; $0.25 < \mathrm{ICC} \le 0.4$ indicated low reliability; $0.4 < \mathrm{ICC} \le 0.6$ indicated fair reliability; $0.6 < \mathrm{ICC} \le 0.75$ showed that reliability was good; and $0.75 < \mathrm{ICC} \le 1.0$ meant that reliability was excellent, close to perfect. We usually expect a fair to almost perfect reliability index ($\mathrm{ICC} > 0.4$).

2.7 | Classification analysis

To classify subjects into HC and patients using ROI-based BENs, a linear support vector machines (SVM) approach was implemented (Dosenbach et al., 2010). SVMs have supervised learning models which can be used for classification tasks (Cortes & Vapnik, 1995).

Given labeled training data with n features, the algorithm outputs an optimal hyperplane that can separate the classes with a maximal margin. Subjects were separated into stratified training (90%) and test (10%) subsets for each HC and disease dataset. The same training and test subsets were used across all atlases so that results could be directly compared with one another. The hyperparameter tuning of penalty parameter C was conducted using nested cross-validation in which both the inner and outer folds were randomly split into five stratified groups. A single best model and the hyperparameter C corresponding to it were identified. This nested grid search cross-validation was repeated 100 times to generate 100 different values for C. The final model was created by averaging the hyperparameter C obtained across 100 iterations of the more acceptable grid search. This final model was evaluated on the test subset, and the corresponding accuracy, the area under the receiver operating characteristics curve, and feature importance are reported. This was repeated using the same 10 permutations of randomized training and testing splits to distribute overall performance metrics for BEN classification.

2.8 | Node definition

Considering that different atlases will affect the analysis results, three atlases are used in this paper, namely the Brainnetome atlas (Fan et al., 2016), the Dosenbach atlas (Dosenbach et al., 2010), and the Power atlas (Power et al., 2011), shown in Figure 2. By comparing the differences between different atlases and finding no significant difference, the results obtained in this paper can be said to be atlas independent.

3 | RESULTS

3.1 | Reliability comparison of different BENs

In this part, we use rs-fMRI data with 10 sessions from the MSC dataset to explore the reliability of different BENs, in Figures 3 and 4. Additionally, we simulated and generated three distributed random sequences, calculated their entropy, and then explored the reliability of the different entropies, in Figure 5.

In Step 1, extracted ROIs within DMN in the Dosenbach atlas (Dosenbach et al., 2010) and calculated the BENs of the extracted rs-fMRI data using the seven entropy methods mentioned above. Each session of rs-fMRI was calculated to obtain session BENs of nine subjects in total.

In Step 2, we calculated the ICC of the repeated sessions with the data obtained from *Step* 1.

In Step 3, we select $k = [3, 6, 10]$ (k means how many rs-fMRI sessions were used) to test BEN's reproducing reliability, and Figure 3 shows the distribution of ICC values.

In Figure 4, we also performed a two-sample t-test on different entropy methods when $k = 10$ to see whether there is a significant difference between methods. This proves that the ICC values vary when calculated by different entropy methods. The results displayed on the three templates are consistent; that is, the reliability of DiffEn was better than those of the other entropy methods, regardless of the template used. From Figure 3, DiffEn is more stable when the number of sessions increases and has the highest average ICC value. Based on Figure 4, the two-sample t-test showed a significant difference among entropy methods. Furthermore, the performance is consistent with no significant difference during these three atlases, namely the Brainnetome atlas (Fan et al., 2016), the Dosenbach atlas (Dosenbach et al., 2010), and the Power atlas (Power et al., 2011).

From theoretical knowledge, if multiple time series meet the same probability density distribution, although the entropy values calculated using different methods may be different, the entropy values calculated using the same method should be the same. If the same entropy were calculated repeatedly for time-series possessing different probability density distributions, the obtained entropy values would be different. Moreover, to further test the difference between entropy methods, we calculate seven types of entropy on three simulation time-series with different types of distribution: Normal, Rayleigh, and Weibull distribution time series using MATLAB (2016b) software. The size of each simulation time series is 160×100, where 160 and 100 represent the number of regions and length of the time series, respectively, and the results are shown in Figure 5. In this part, since the time series of 160 brain regions are generated using the same probability density distribution function, the entropy of the 160 brain regions is the same. From Figure 5, no matter what kind of distribution the simulated time series have, DiffEn demonstrates relatively minor fluctuations. Therefore, since the results above show the reliability of BENs and present the differences between each entropy method, it makes sense to illustrate which entropy method is the most reliable and valid in extracting brain features.

3.2 | Altered complexity of spontaneous brain activity

In this part, we classified ADHD, BP, and SCHZ using BEN obtained from the seven entropy methods mentioned above. Before the classification task, we first performed a two-sample t-test between HC and patients on ROI levels. Figure 6 exhibits the results of the two-sample t-test between HC and different diseases. Based on Figure 6, Tables 1–3 show how many ROIs significantly differ between HC and three diseases (ADHD, BP, and SCHZ). For ADHD, we find a difference between HC and ADHD, mainly in the DMN and sensorimotor network. For BP, different regions between HC and BP include mainly the DMN, sensorimotor, and frontoparietal networks. For SCHZ, the different regions between HC and SCHZ are mainly sensorimotor and cingulo-opercular. In addition, DiffEn is good at exploring the similarities and differences between ADHD, BP, SCHZ, and HC. Likewise, by comparing the differences between different atlases and finding no significant difference, the results obtained in this article are atlas independent.

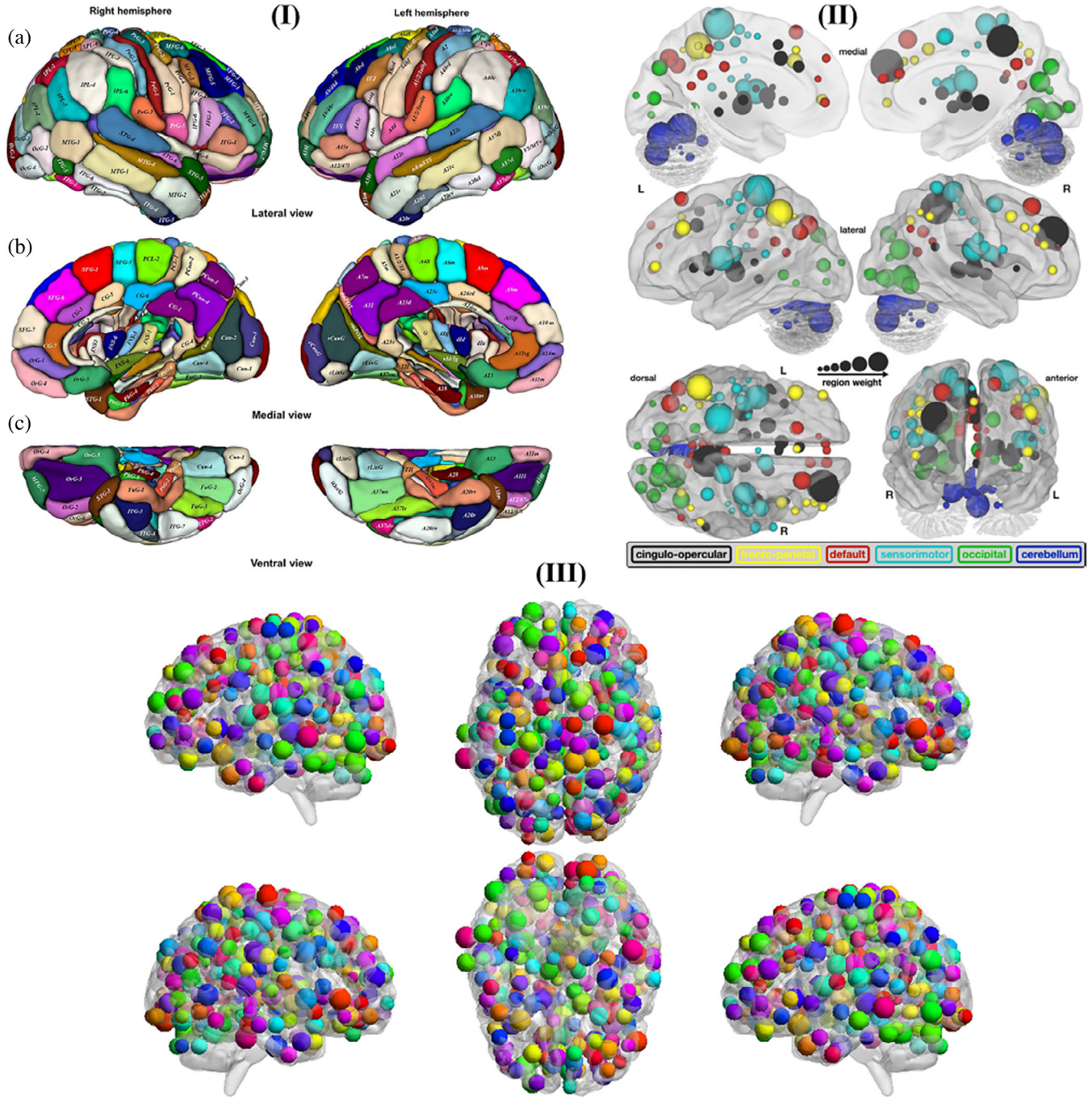

FIGURE 2 Functional connectivity multivariate pattern analysis region (node) weights. (I) Parcellation scheme of the human brain in the Brainnetome atlas (Fan et al., 2016). The MPM for each of the cortical subregions was created in standard MNI space visualized using ITK-SNAP (www.itksnap.org); (II) the ROIs are color-coded according to the six identified functional networks (Dosenbach et al., 2010); (III) Power atlas (Power et al., 2011): The figure was generated with BrainNet viewer (Csermely et al., 2013)

Specifically, from Table 1, based on the Dosenbach atlas, we found that ApEn, DispEn, and PeEn are not suitable for studying the difference between ADHD and HC because they could not identify the altered regions between HC and ADHD. The other four entropies may be more suitable for finding different brain regions (ADHD, HC). Among them, DiffEn found the most different amount of brain regions within a network (DMN: 8, sensorimotor:26, occipital: 10, frontoparietal: 8, cingulo-opercular: 18, and cerebellum: 12), followed by FuEn (DMN: 5, sensorimotor: 18, occipital: 8, frontoparietal: 7, cingulo-opercular: 16, and cerebellum:9), RaEn (DMN: 6, sensorimotor: 16, occipital: 7, frontoparietal: 6, cingulo-opercular: 15, and cerebellum: 5), and the least was SaEn (DMN: 4, sensorimotor: 14, occipital: 3, frontoparietal: 6, cingulo-opercular: 8, and cerebellum: 7). Based on the results of BEN, the sensorimotor network changed

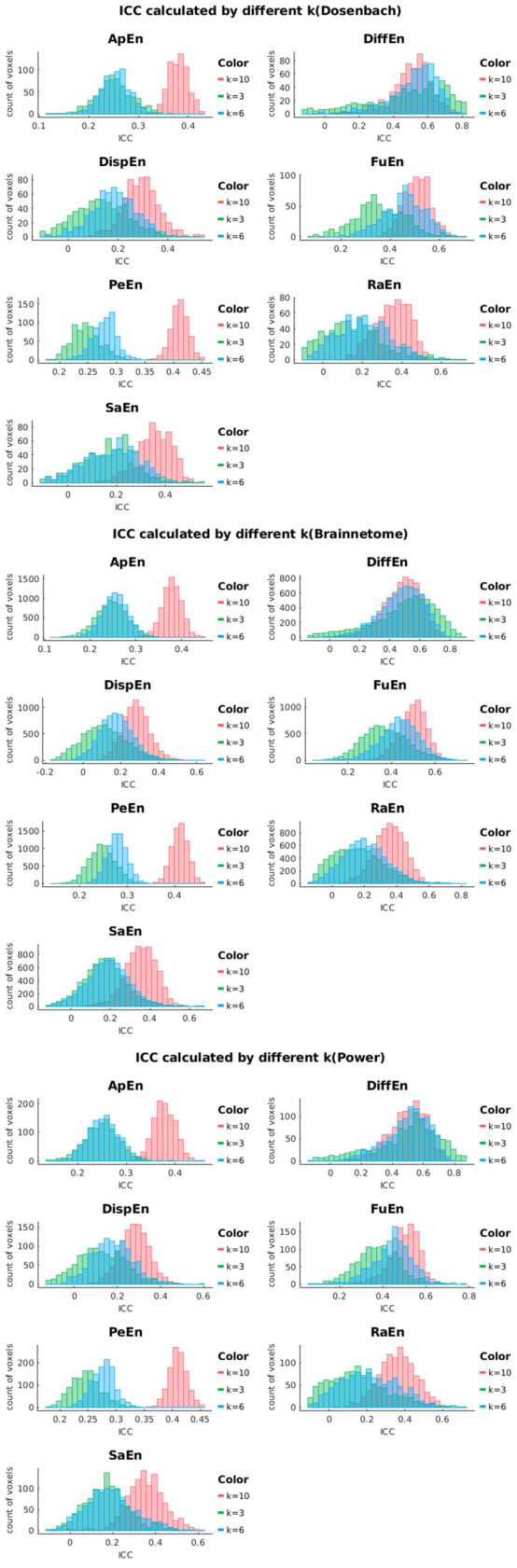

FIGURE 3 Comparison ICC for different BENs with three types number sessions in DMN shown in Brainnetome atlas, Dosenbach atlas, and Power atlas, *k* means how many sessions were used

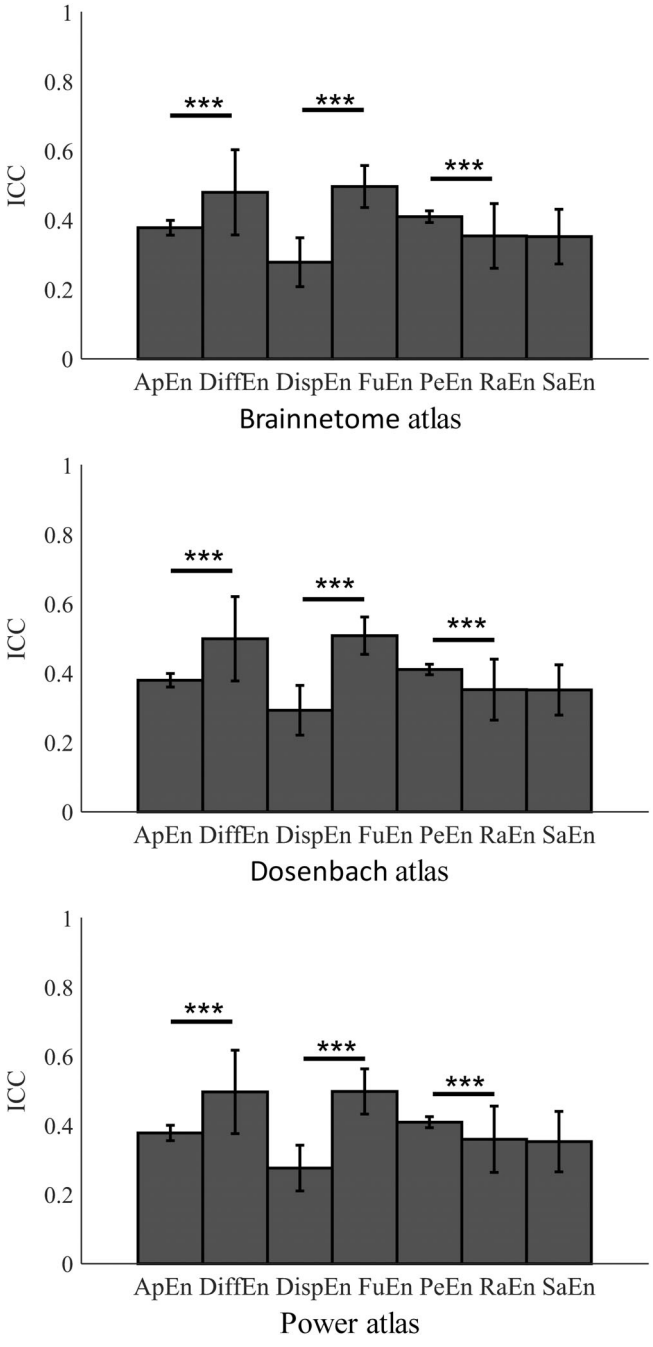

FIGURE 4 Performance of a two-sample *t*-test on different entropy methods when $k = 10$ (*$p < .05$, **$p < .01$, ***$p < .001$), *k* means that how many sessions were used

greatly, and DMN, occipital, and cingulo-opercular changed more so than the cerebellum.

From Table 2, based on the Dosenbach atlas, we found that ApEn, DispEn, and PeEn cannot identify the altered regions between HC and BP. DiffEn, FuEn, RaEn, and SaEn seem to find many different brain regions (BP, HC). Among them, DiffEn found the highest number of different brain regions (DMN: 11, sensorimotor: 18, occipital:

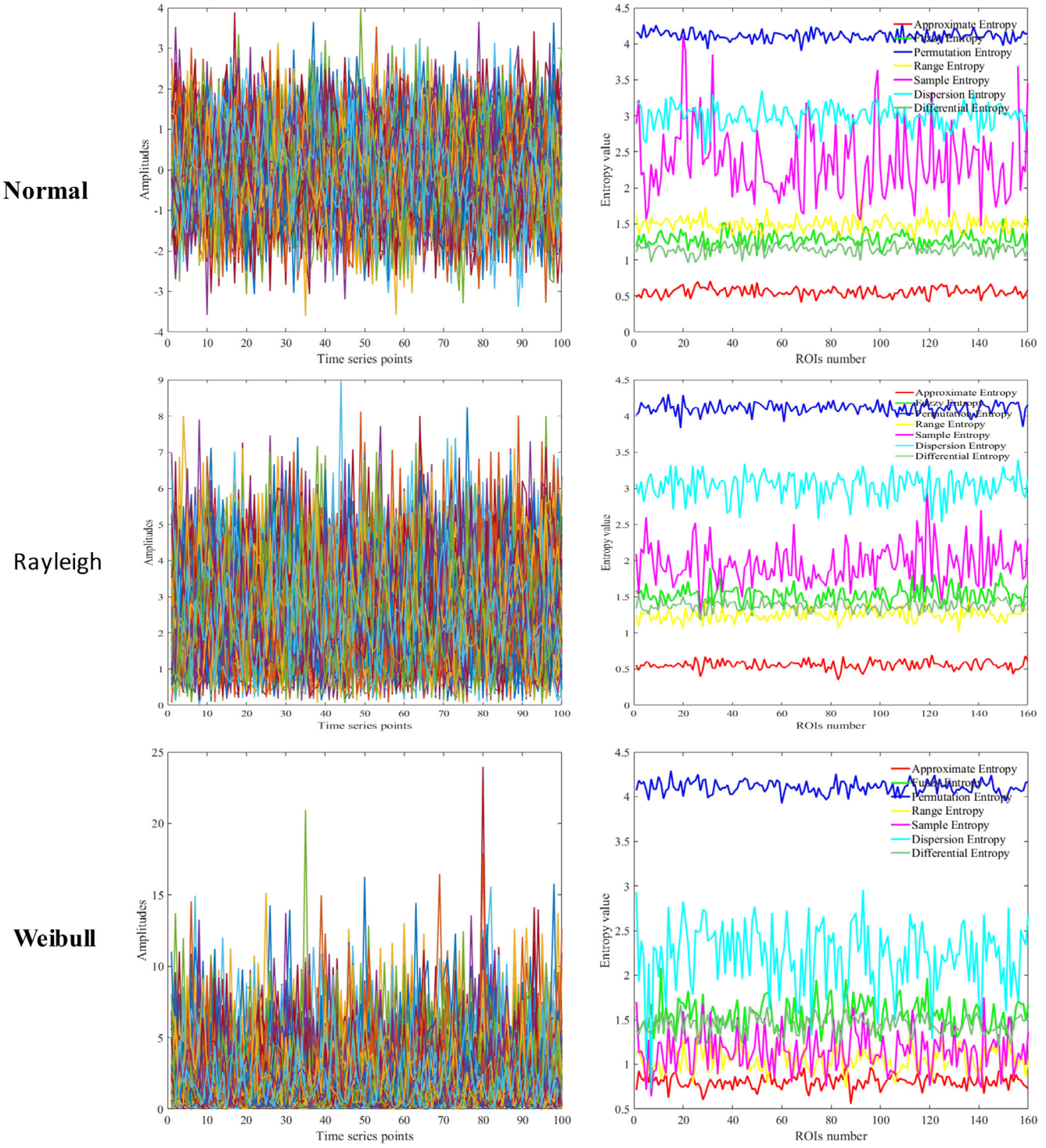

FIGURE 5 Entropy performance results of simulation time-series. *First column*: simulation time-series follows Normal distribution (random ["Normal",0,1,160,100]), Weibull distribution (random["Weibull",2,1,160,100]), and Rayleigh distribution (random["Rayleigh",2,160,100]); *second column*: entropy values were calculated by using seven entropy methods; *first row*: when data follows Normal distribution, all the entropy methods show a stable curve except SaEn; *second row*: when data follow Weibull distribution, all the entropy methods show a stable curve except SaEn; *third row*: when data follows Rayleigh distribution, all the entropy methods show a stable curve except DispEn

8, frontoparietal: 12, cingulo-opercular: 14, and cerebellum: 7), followed by FuEn (DMN: 10, sensorimotor: 15, occipital: 5 frontoparietal: 11, cingulo-opercular: 13, and cerebellum: 10), and SaEn (DMN: 10, sensorimotor: 10, occipital: 3 frontoparietal: 9, cingulo-opercular: 10, and cerebellum: 4) and the least was RaEn (DMN: 6, sensorimotor: 9, occipital: 1 frontoparietal: 5, cingulo-opercular: 7, and cerebellum: 2). Based on the results of BEN, sensorimotor and DMN networks changed significantly.

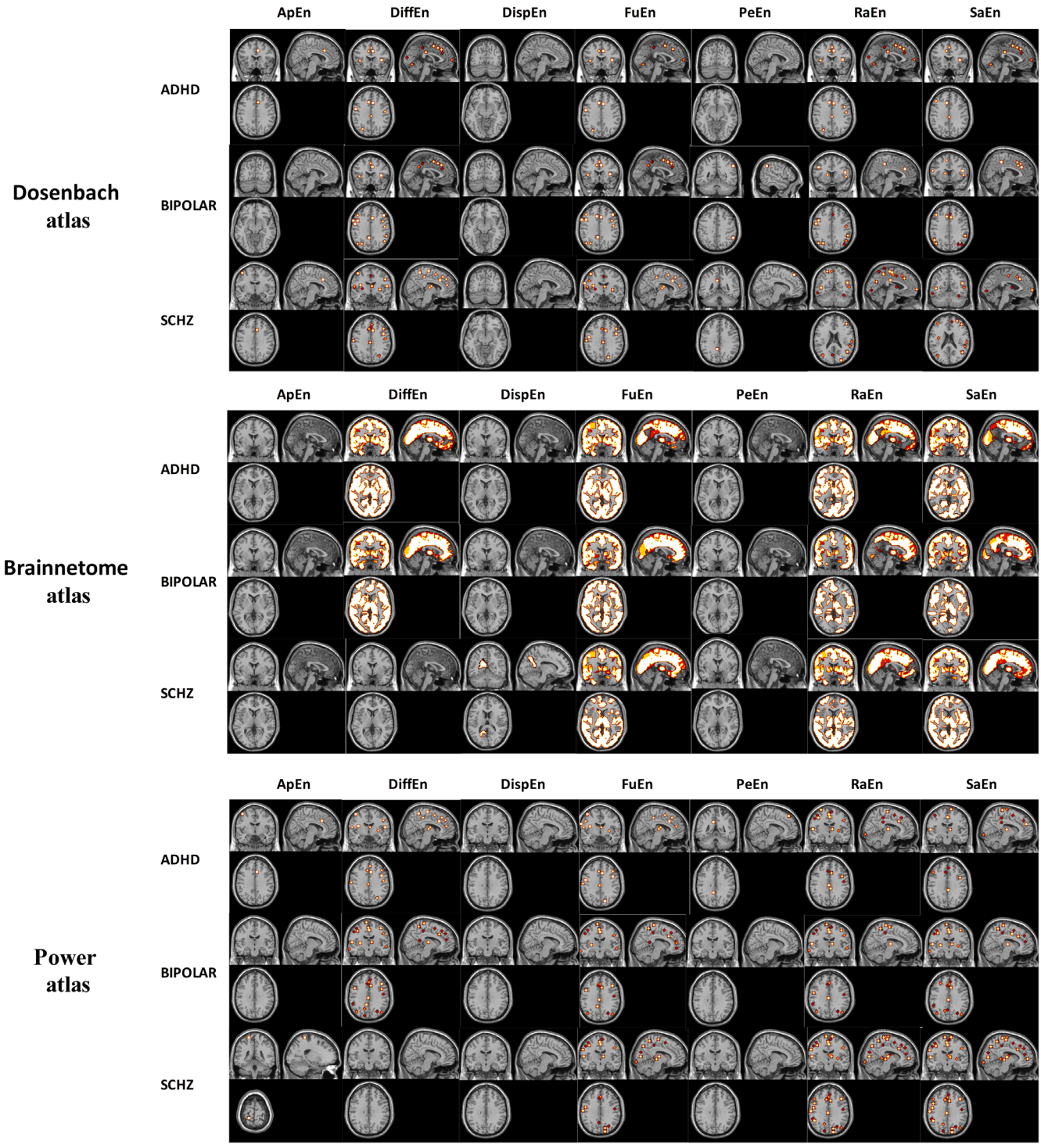

FIGURE 6 Slice images of the brain regions with significant differences between HC and patient. The number of specific brain regions with significant differences is shown in Tables 1–4

From Table 3, based on the Dosenbach atlas, we found that ApEn, DiffEn, DispEn, and PeEn cannot identify the altered regions between HC and SCHZ. SaEn, RaEn, and FuEn seem to find many different brain regions (SCHZ, HC). Among them, SaEn found the highest number of different brain regions (DMN: 12, sensorimotor: 23, occipital: 11, frontoparietal: 8, cingulo-opercular: 13, and cerebellum: 9), followed by RaEn (DMN: 12, sensorimotor: 20, occipital: 15, frontoparietal: 5, cingulo-opercular: 12, and cerebellum: 6), and the least was FuEn (DMN: 3, sensorimotor: 19, occipital: 14, frontoparietal: 2, cingulo-opercular: 11, and cerebellum: 10). Based on the results of DiffEn, sensorimotor and DMN networks changed the most, with frontoparietal and cingulo-opercular networks changing more than the occipital network.

Similar meaningful results are seen for each condition based on the described above. These three disorders share brain regions that show significant change compared to HC. Whole regions are changed, and the sensorimotor network, in particular, changes noticeably in all disorders. However, other regions do not show the same degrees of change, specifically for ADHD where cingulo-opercular > (occipital DMN, frontoparietal). For BP, cingulo-opercular > (occipital, DMN, frontoparietal). For SCHZ (cingulo-opercular, DMN, occipital) > frontoparietal. Furthermore, Figure 6 is slice images of the brain regions with significant differences between HC and patient. It is worth noting that a similar pattern is obtained on the Brainnetome atlas and the Power atlas based on the Dosenbach atlas. That is to say, the conclusion is not affected by the atlas.

3.3 | Multiscale entropy analysis

For each atlas, we extracted the average multiscale entropy to ROIs. For each ROI, the differences in multiscale entropy values among the three groups were compared using an independent samples *t*-test, and *p* values are listed in Table 4. The average multiscale entropy values in all ROIs over multiple time scales for the four groups (ADHD, BP, SCHZ, and HC) are shown in Figure 7. Regardless of the atlas used, the mean multiscale entropy values for the ADHD, BP, and SCHZ were significantly lower than for the HCs (both *p*-value <.05). More detailed results are presented in Table 4. Besides, it is also found that the performance of different multiscale entropy algorithms on different diseases is also different, such as DiffEn, RaEn, and SaEn performed better in ADHD, SCHZ, and BP, respectively.

3.4 | Classification comparison of different BENs

When a two-sample t-test was done, we did a classification task based on entropy values calculated using different ROI levels and the whole brain based on three different atlases. The result is presented in Tables 5 and 6. Table 5 shows the classification results at the whole-brain level from the three atlases studies. From the ADHD classification results, it can be seen that DiffEn performs the best, where DiffEn achieves an accuracy of 0.8548. Among the classification results of BP, SaEn performs the best, where SaEn achieves an accuracy of 0.8824. For the classification results of SCHZ, RaEn performs

TABLE 1 Counting the ROIs which have a significant difference between HC and ADHD (num_of_diff_area refers to the number of ROIs which significantly differ from HC and ADHD)

		num_of_diff_area	Default	Sensorimotor	Occipital	Frontoparietal	Cingulo-opercular	Cerebellum
Dosenbach atlas	ApEn	1	0	0	0	0	1	0
	DiffEn	82	8	26	10	8	18	12
	DispEn	0	0	0	0	0	0	0
	FuEn	63	5	18	8	7	16	9
	PeEn	0	0	0	0	0	0	0
	RaEn	55	6	16	7	6	15	5
	SaEn	42	4	14	3	6	8	7

		num_of_diff_area	Visual	Ensorimotor	Dorsal attention	Ventral attention	Limic	Frontoparietal	Default
Brainnetome atlas	ApEn	0	0	0	0	0	0	0	0
	DiffEn	184	29	33	30	22	16	22	32
	DispEn	0	0	0	0	0	0	0	0
	FuEn	165	27	32	27	22	12	21	24
	PeEn	0	0	0	0	0	0	0	0
	RaEn	107	23	29	25	19	10	20	21
	SaEn	130	20	27	21	19	6	17	20

		num_of_diff_area	SMN	AN	CON	DMN	VN	FPN	SN	SCN	VAN	DAN
Power atlas	ApEn	3	1	0	1	0	0	0	0	0	0	1
	DiffEn	98	18	9	7	11	13	8	9	11	5	7
	DispEn	0	0	0	0	0	0	0	0	0	0	0
	FuEn	77	15	7	6	8	15	7	3	6	4	6
	PeEn	3	0	0	0	2	0	0	0	0	0	1
	RaEn	71	15	7	7	7	9	6	5	7	4	4
	SaEn	51	8	5	3	8	5	7	6	5	2	2

TABLE 2 Counting the ROIs which have a significant difference between HC and BP (num_of_diff_area refers to the number of ROIs which significantly differ from HC and BP)

		num_of_diff_area	Default	Sensorimotor	Occipital	Frontoparietal	Cingulo-opercular	Cerebellum
Dosenbach atlas	ApEn	0	0	0	0	0	0	0
	DiffEn	70	11	18	8	12	14	7
	DispEn	0	0	0	0	0	0	0
	FuEn	64	10	15	5	11	13	10
	PeEn	1	0	0	0	1	0	0
	RaEn	30	6	9	1	5	7	2
	SaEn	46	10	10	3	9	10	4

		num_of_diff_area	Visual	Sensorimotor	Dorsal attention	Ventral attention	Limic	Frontoparietal	Default
Brainnetome atlas	ApEn	0	0	0	0	0	0	0	0
	DiffEn	176	28	29	28	21	14	23	33
	DispEn	0	0	0	0	0	0	0	0
	FuEn	176	25	28	29	20	15	24	35
	PeEn	0	0	0	0	0	0	0	0
	RaEn	114	16	19	16	16	13	13	21
	SaEn	122	24	20	17	18	6	13	24

		num_of_diff_area	SMN	AN	CON	DMN	VN	FPN	SN	SCN	VAN	DAN
Power atlas	ApEn	0	0	0	0	0	0	0	0	0	0	0
	DiffEn	108	25	2	8	20	14	13	10	3	6	7
	DispEn	0	0	0	0	0	0	0	0	0	0	0
	FuEn	90	21	0	8	17	11	12	7	2	6	6
	PeEn	0	0	0	0	0	0	0	0	0	0	0
	RaEn	57	21	1	4	8	6	3	4	2	3	5
	SaEn	87	20	1	9	21	8	7	8	6	2	5

the best, where RaEn achieves an accuracy of 0.8409. Refer to Table 5 for details. Table 6 is based on the best results of a whole-brain classification in Table 5.

The weights of the corresponding linear kernel SVM classifiers are analyzed to explore the critical brain regions that affect ADHD, BP, and SCHZ. Among them, DiffEn achieves an accuracy of 0.8548. Among the classification results of BP, SaEn performs the best, where SaEn achieves an accuracy of 0.8824. For the classification results of SCHZ, RaEn performs the best, where RaEn achieves an accuracy of 0.8409. Please refer to Table 5 for details. Specifically, for ADHD, DiffEn (accuracy = 0.8548) was used in this experiment as a means of weight analysis.

The top 10 key features (brain regions) of the weight ranking of DiffEn corresponding classifier were L_Lateral Occipital Cortex, superior division, R_Supramarginal Gyrus, anterior division, L_Cuneal Cortex, L_Occipital Pole, R_Cuneal Cortex, L_Postcentral Gyrus, L_Cuneal Cortex, R_Cingulate Gyrus, posterior division, L_Inferior Temporal Gyrus, temporooccipital part, and L_Frontal Pole, respectively. For BP, this experiment uses SaEn (accuracy = 0.8824) to analyze weights. The top 10 key features (brain regions) of the weights of the classifiers corresponding to SaEn are L_Middle Temporal Gyrus, posterior division, R_Middle Frontal Gyrus, R_Middle Temporal Gyrus, posterior division, R_Frontal Medial Cortex, L_Frontal Pole, R_Precentral Gyrus, R_Temporal Fusiform Cortex, posterior division, R_Postcentral Gyrus, L_Lateral Occipital Cortex, superior division, R_Lateral Occipital Cortex, and inferior division. For SCHZ, this experiment uses RaEn (accuracy = 0.8409) as analysis weight. The top 10 key features (brain areas) of the classifiers corresponding to RaEn are: L_Frontal Pole, R_Superior Temporal Gyrus, posterior division, R_Angular Gyrus, R_Frontal Pole, L_Frontal Pole, L_Frontal Pole, R_Supramarginal Gyrus, posterior division, R_Supramarginal Gyrus, posterior division, R_Frontal Orbital Cortex, and L_Frontal Pole. For details, refer to Table 6.

4 | DISCUSSION

The similarities and differences between ADHD, BP, and SCHZ are fascinating research topics, and entropy theory is a suitable method for exploring the complexity of time series from a nonlinear perspective. So, is it possible to find a reliable and effective entropy method to reveal the similarities and differences among ADHD, BP, and SCHZ. This article calculated and analyzed the ICC of seven kinds of entropy using the MSC dataset and simulation data; the results displayed on

TABLE 3 Counting the ROIs which have a significant difference between HC and SCHZ (num_of_diff_area refers to the number of ROIs which significantly differ from HC and SCHZ)

		num_of_diff_area	Default	Sensorimotor	Occipital	Frontoparietal	Cingulo-opercular	Cerebellum
Dosenbach atlas	ApEn	0	0	0	0	0	0	0
	DiffEn	0	0	0	0	0	0	0
	DispEn	0	0	0	0	0	0	0
	FuEn	59	3	19	14	2	11	10
	PeEn	0	0	0	0	0	0	0
	RaEn	70	12	20	15	5	12	6
	SaEn	76	12	23	11	8	13	9

		num_of_diff_area	Visual	Sensorimotor	Dorsal attention	Ventral attention	Limic	Frontoparietal	Default
Brainnetome atlas	ApEn	0	0	0	0	0	0	0	0
	DiffEn	0	0	0	0	0	0	0	0
	DispEn	1	1	0	0	0	0	0	0
	FuEn	141	30	31	21	14	8	11	26
	PeEn	0	0	0	0	0	0	0	0
	RaEn	148	31	31	20	12	14	16	24
	SaEn	154	29	33	26	17	5	18	26

		num_of_diff_area	SMN	AN	CON	DMN	VN	FPN	SN	SCN	VAN	DAN
Power atlas	ApEn	1	1	0	0	0	0	0	0	0	0	0
	DiffEn	0	0	0	0	0	0	0	0	0	0	0
	DispEn	0	0	0	0	0	0	0	0	0	0	0
	FuEn	70	24	3	2	2	24	0	4	4	2	7
	PeEn	0	0	0	0	0	0	0	0	0	0	0
	RaEn	112	30	7	5	11	25	4	8	10	5	7
	SaEn	117	30	7	5	14	26	8	8	8	3	8

the three templates are consistent; that is, the reliability of DiffEn was better than those of the other entropy methods. Then, we used seven kinds of entropy and multiscale entropy expanded based on seven kinds of entropy to explore the differences between brain regions. We found a difference between HC and ADHD, BP, SCHZ, specifically, cingulo-opercular > (occipital DMN and frontoparietal) in ADHD, cingulo-opercular > (occipital, DMN, and frontoparietal) in BP, (cingulo-opercular, DMN, and occipital) > frontoparietal in SCHZ. Also, the same regions are significantly changed between ADHD, BP, and SCHZ focusing on "pre-SMA," "dlPFC_2," "vFC_3," and "ant_insula_2." Further, regardless of the atlas used, the mean multiscale entropy values for the ADHD, BP, and SCHZ were significantly lower than for the HCs. Besides, it is also found that different multiscale entropy algorithms on different diseases are also different, such as DiffEn, RaEn, and SaEn performed better in ADHD, SCHZ, and BP, respectively. By verifying the classification performance of the seven information entropies on ADHD, BP, and SCHZ, the effectiveness of the seven entropy methods is evaluated, and the ADHD classification results can be seen that DiffEn performs the best, where DiffEn achieves an accuracy of the 0.8548. Among the classification results of BP, SaEn performs the best, where SaEn achieves an accuracy of 0.8824. For the classification results of SCHZ, RaEn performs the best, where RaEn achieves an accuracy of 0.8409. Besides, for details, the top 10 key brain regions of the weight ranking of entropy corresponding to SVM of each disease list in Table 6. The regions with the most significant differences include the DMN, sensorimotor, and visual networks. The patients have impaired DMN and changes in sensorimotor and visual regions. Next, we will thoroughly discuss and cite the research results of the existing public literature and then support the accuracy of the results of this article.

4.1 | The entropy method comparison

The multiscale entropy is obtained only by scale expansion on the single-scale entropy, and then the complexity of sequence or topology can be studied from different scales (Costa et al., 2005; Ferraz & Kihara, 2022; Marinazzo et al., 2020). The core of different multiscale entropy is the single-scale entropy, so it is necessary to discuss the difference in single-scale entropy. In physiological signal analysis, ApEn and SaEn are two of the most commonly used measures. SaEn is an improved version of ApEn and aims to overcome the limitations of ApEn and reduce statistical bias (Richman & Moorman, 2000). However, both measures still suffer from sensitivity to signal

TABLE 4 *p*-value when doing *t*-test between HC and patient under each scale in multiscale entropy

			Scale1	Scale2	Scale3	Scale4	Scale5	Scale6	Scale7	Scale8	Scale9	Scale10
Dosenbach Atlas	ApEn	ADHD versus HC	5.42 E−01	0.862778	0.681854	1.70 E−01	1.52 E−02	5.90 E−02	9.22 E−05	3.15 E−05	1.26 E−11	6.44 E−07
		BP versus HC	4.54 E−01	0.958768	2.91 E−01	2.09 E−01	1.36 E−02	1.01 E−04	9.73 E−06	2.17 E−03	6.46 E−10	4.41 E−06
		SCHZ versus HC	0.096719	1.57 E−01	0.000857	2.18 E−07	4.99 E−12	1.75 E−05	9.22 E−09	9.91 E−06	1.68 E−06	2.45 E−06
	DiffEn	ADHD versus HC	0	0	0	0	0	0	0	0	0	0
		BP versus HC	0	0	0	0	0	0	0	0	0	0
		SCHZ versus HC	2.56 E−06	2.17 E−06	1.31 E−06	1.37 E−06	5.54 E−07	8.08 E−07	6.22 E−07	2.02 E−07	1.94 E−07	1.99 E−07
	DispEn	ADHD versus HC	0.87122	0.932104	0.881494	0.867574	0.860153	0.979924	0.872463	0.955229	0.963569	0.829123
		BP versus HC	0.710197	0.629743	5.32 E−01	0.743821	0.771877	0.927772	0.747181	0.92423	0.929188	0.664302
		SCHZ versus HC	0.09161	0.090982	0.069054	0.073075	0.07336	0.129972	0.114045	0.189354	5.69 E−01	5.54 E−01
	FuEn	ADHD versus HC	0	0	0	0	0	0	0	0	0	0
		BP versus HC	0	0	0	0	0	0	0	0	0	0
		SCHZ versus HC	0	0	0	0	0	0	0	0	0	0
	PeEn	ADHD versus HC	0.980014	0.945064	8.64 E−01	0.972537	0.996409	0.970417	0.983851	0.914109	0.901527	0.973003
		BP versus HC	0.976955	8.95 E−01	8.86 E−01	0.90943	0.998726	0.953171	0.98879	0.953927	0.959342	0.954549
		SCHZ versus HC	0.970866	0.963723	9.17 E−01	0.993631	0.986078	0.933668	0.952259	0.990491	0.958617	0.942285
	RaEn	ADHD versus HC	0	0	0	0	0	0	0	0	0	0
		BP versus HC	0	0	0	0	0	0	0	0	0	0
		SCHZ versus HC	0	0	0	0	0	0	0	0	0	0
	SaEn	ADHD versus HC	0.983539	0.804394	0.485762	0.243748	0.568504	0.134892	0.008929	2.37 E−02	5.54 E−03	0.001143
		BP versus HC	0.727117	0.92264	0.71321	0.785789	0.303471	0.017254	0.001032	0.225901	0.016572	0.008635
		SCHZ versus HC	3.69 E−02	1.49 E−01	0.556843	0.122292	0.012801	0.007349	0.000127	0.017705	0.038067	0.003186
Brainnetome Atlas	ApEn	ADHD versus HC	7.87 E−14	0.00095	0.025687	1.69 E−12	4.67 E−09	1.18 E−11	5.85 E−07	1.11 E−16	0	3.33 E−16
		BP versus HC	0	0.835699	6.99 E−11	2.08 E−11	6.02 E−10	0	3.55 E−15	0	0	0
		SCHZ versus HC	0	5.20 E−06	0	0	0	0	0	0	0	2.22 E−16
	DiffEn	ADHD versus HC	0	0	0	0	0	0	0	0	0	0
		BP versus HC	0	0	0	0	0	0	0	0	0	0
		SCHZ versus HC	2.33 E−13	1.65 E−13	6.36 E−14	7.15 E−14	1.80 E−14	1.77 E−14	1.71 E−14	1.44 E−15	6.66 E−16	1.33 E−15
	DispEn	ADHD versus HC	0.63421	0.391857	0.087307	0.049662	0.125646	0.000372	0.891031	0.255557	0.049267	0.000209
		BP versus HC	0.000305	1.70 E−05	1.60 E−12	0.000117	0.049124	0.01781	0.065422	0.686835	0.14591	0.002972
		SCHZ versus HC	0	0	0	0	0	0	0	0	2.15 E−12	4.11 E−13
	FuEn	ADHD versus HC	0	0	0	0	0	0	0	0	0	0
		BP versus HC	0	0	0	0	0	0	0	0	0	0
		SCHZ versus HC	0	0	0	0	0	0	0	0	0	0

(Continues)

TABLE 4 (Continued)

			Scale1	Scale2	Scale3	Scale4	Scale5	Scale6	Scale7	Scale8	Scale9	Scale10
	PeEn	ADHD versus HC	0.606011	0.556399	0.000937	0.010093	0.209091	0.808055	0.038417	0.003071	0.713295	0.618626
		BP versus HC	0.000598	0.004971	9.61 E−10	0.001702	0.680806	0.583516	0.70281	0.060299	0.560629	0.061969
		SCHZ versus HC	0.007967	0.861574	3.78 E−07	0.80384	0.43439	0.002048	0.001721	0.034585	0.002323	0.013266
	RaEn	ADHD versus HC	0	0	0	0	0	0	0	0	0	0
		BP versus HC	0	0	0	0	0	0	0	0	0	0
		SCHZ versus HC	0	0	0	0	0	0	0	0	0	0
	SaEn	ADHD versus HC	0.033689	0.000339	0.16853	0.406284	0.02522	0.905017	0.335832	0.111622	0.000345	0.211443
		BP versus HC	0.039203	0.054795	0.839518	0.004044	0.135037	0.079631	0.8496	0.010689	0.002567	0.949544
		SCHZ versus HC	0	3.65 E−09	0.003218	2.91 E−05	0.003684	0.207161	2.03 E−05	0.297424	0.800837	0.690909
Power Atlas	ApEn	ADHD versus HC	5.05 E−06	0.003769	0.034654	1.96 E−07	1.72 E−10	1.72 E−12	1.47 E−10	0	0	0
		BP versus HC	8.24 E−07	0.312641	1.10 E−05	3.23 E−06	6.38 E−07	8.66 E−15	2.11 E−15	1.74 E−14	0	2.40 E−12
		SCHZ versus HC	0	1.11 E−05	0	0	0	0	0	0	1.11 E−16	1.72 E−12
	DiffEn	ADHD versus HC	0	0	0	0	0	0	0	0	0	0
		BP versus HC	0	0	0	0	0	0	0	0	0	0
		SCHZ versus HC	2.43 E−09	1.85 E−09	9.38 E−10	7.75 E−10	1.93 E−10	3.07 E−10	2.53 E−10	3.43 E−11	3.09 E−11	6.31 E−11
	DispEn	ADHD versus HC	0.023167	0.033965	0.399072	0.048805	0.02567	0.500813	0.070662	0.800918	0.017624	0.247517
		BP versus HC	0.160943	0.003247	4.46 E−07	0.000113	0.08215	0.421923	0.021353	0.026297	0.421556	0.103623
		SCHZ versus HC	0	0	0	0	0	0	0	0	3.11 E−11	8.67 E−07
	FuEn	ADHD versus HC	0	0	0	0	0	0	0	0	0	0
		BP versus HC	0	0	0	0	0	0	0	0	0	0
		SCHZ versus HC	0	0	0	0	0	0	0	0	0	0
	PeEn	ADHD versus HC	0.249469	0.005146	3.36 E−05	0.398779	0.63555	0.616165	0.758724	0.740436	0.478905	0.792394
		BP versus HC	0.01136	4.56 E−06	2.90 E−06	0.002163	0.807999	0.70558	0.71958	0.115011	0.393165	0.252488
		SCHZ versus HC	0.962571	0.148857	2.24 E−09	0.160134	0.462507	0.017787	0.007934	0.810914	0.17836	0.32383
	RaEn	ADHD versus HC	0	0	0	0	0	0	0	0	0	0
		BP versus HC	0	0	0	0	0	0	0	0	0	0
		SCHZ versus HC	0	0	0	0	0	0	0	0	0	0
	SaEn	ADHD versus HC	0.402696	0.644379	0.812666	0.392083	0.248271	0.036421	0.005882	7.05 E−05	1.96 E−05	0.165203
		BP versus HC	0.455469	0.886208	0.387765	0.089462	0.036644	0.066467	0.292789	0.008628	0.126457	0.118451
		SCHZ versus HC	6.66 E−16	8.13 E−08	0.107265	0.000174	0.002655	0.007186	0.000258	0.032267	0.582156	0.118593

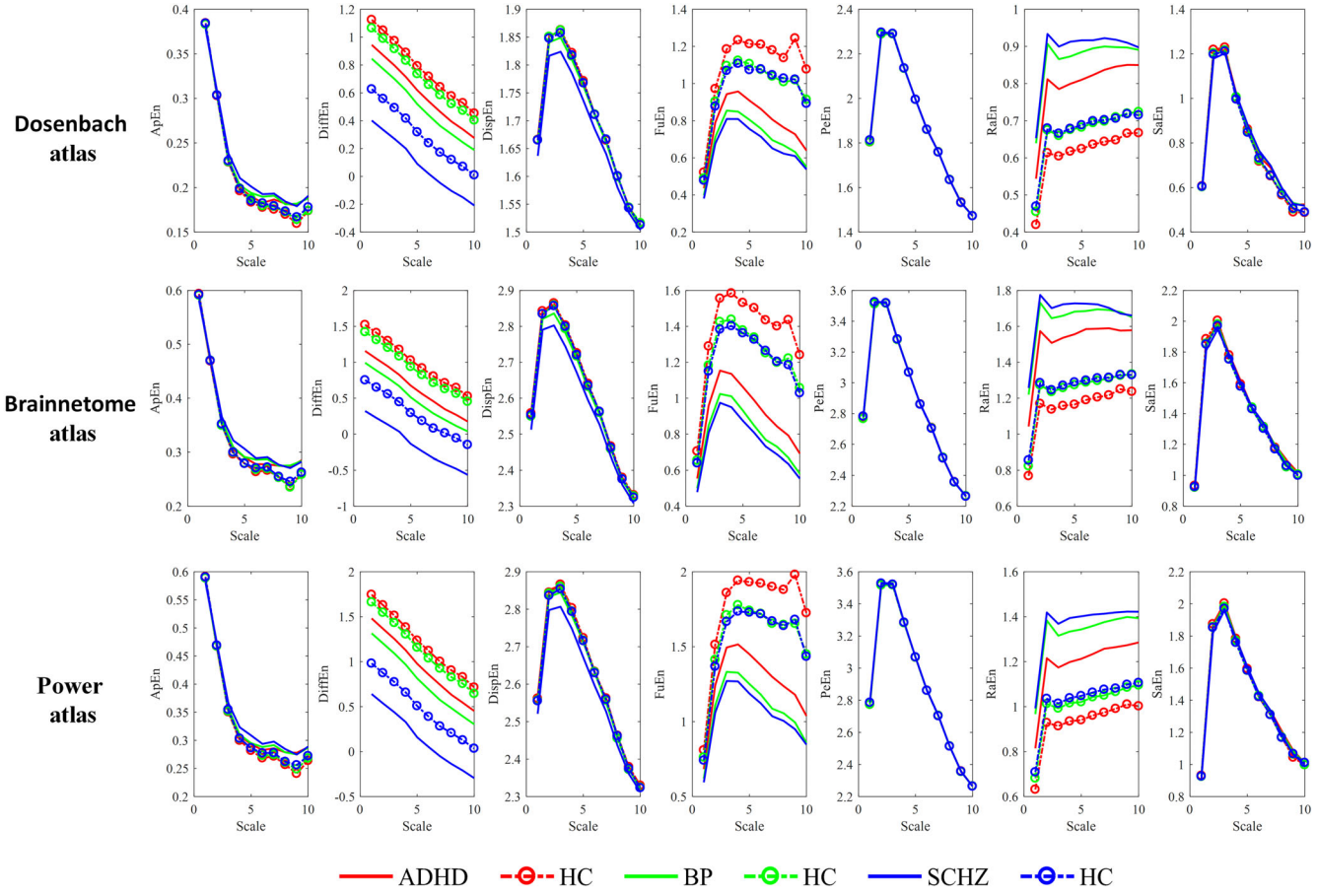

FIGURE 7 Mean multiscale entropy values of gray matter (GM) in the ADHD, BP, SCHZ, and HC

amplitude changes, so, Chen et al. (2007) proposed the FuEn, which is an improvement over the ApEn and SaEn algorithms. As another widely used entropy measure, PeEn is a novel method developed by Bandt to characterize the complexity of time series (Bandt & Pompe, 2002). Although PeEn is conceptually simple and computationally fast, PeEn does not consider the mean value of amplitudes and the differences between amplitude values (Rostaghi & Azami, 2016). RaEn (Omidvarnia et al., 2018) is a proposed modification to ApEn and SaEn, which are highly sensitive to signal amplitude changes and less affected by variation in the magnitude of signals. DispEn (Rostaghi & Azami, 2016) originates from SaEn and PeEn, which can detect the noise bandwidth and simultaneous frequency and amplitude change. It does not lead to undefined results in short signals, is less sensitive to noise, and is considerably faster than SaEn. DiffEn (Duan et al., 2013) measures the complexity of a continuous random variable, is the entropy of a continuous random variable, and is also related to minimum description length. Besides, rs-fMRI signals maybe include multi-type noises, complex nonlinear (Guan et al., 2020), and fractal structures (Guan et al., 2022). Therefore, if some entropy methods can be less sensitive to noise or highly sensitive to signal amplitude changes and less affected by variation in the magnitude of signals, then these entropy methods should be able to show good performance. The results of the ICC of seven kinds of entropy using the MSC dataset and simulation data displayed on the three templates are consistent, and the reliability of DiffEn was better. The core brain regions that affect the classification are given, and DiffEn performed best on ADHD, SaEn for BP, and RaEn for SCHZ.

4.2 | The variation of the complexity

4.2.1 | ADHD and HC

Several studies have shown a downward trend in brain complexity in visual brain regions in ADHD compared with HC (Akdeniz, 2017; Sokunbi et al., 2013). A meta-analytical study suggests that ADHD-related dysfunction is associated with multiple neuronal systems involved in higher-order cognitive functions and sensorimotor processes, including the visual system and the DMN (Cortese et al., 2012). Cortese and colleagues found ADHD-related hyperactivation in the visual network and the DMN (Cortese et al., 2012). Furthermore, Sutcubasi and colleagues (Sutcubasi et al., 2020) found that ADHD was associated with a connectivity disruption within the DMN than HC. Sun and colleagues (Sun et al., 2020) found that regions of the DMN and sensorimotor network were altered in ADHD compared with HC by comparing local consistency in ADHD and HC. In addition,

TABLE 5 Whole-brain level: Classification result

	Dataset	Indice\method	ApEn	DiffEn	DispEn	FuEn	PeEn	RaEn	SaEn
Dosenbach atlas	ADHD	acc	0.5968	**0.8065**	0.2903	0.7097	0.5323	0.6774	0.7419
		Sensitivity	0.5161	**0.8065**	0.2258	0.7742	0.4194	0.7419	0.7419
		Specificity	0.6774	**0.8065**	0.3548	0.6452	0.6452	0.6129	0.7419
		auc	0.5968	**0.8065**	0.2903	0.7097	0.5323	0.6774	0.7419
	BP	acc	0.3971	0.7647	0.3235	0.7941	0.4559	0.7353	**0.8235**
		Sensitivity	0.3235	0.7941	0.3235	0.8824	0.3824	0.7353	**0.7647**
		Specificity	0.4706	0.7353	0.3235	0.7059	0.5294	0.7353	**0.8824**
		auc	0.3971	0.7647	0.3235	0.7941	0.4559	0.7353	**0.8235**
	SCHZ	acc	0.5682	0.6932	0.7159	**0.7727**	0.5682	**0.6932**	0.7159
		Sensitivity	0.5909	0.7955	0.5682	**0.8636**	0.5682	**0.7273**	0.6818
		Specificity	0.5455	0.5909	0.8636	**0.6818**	0.5682	**0.6591**	0.75
		auc	0.5682	0.6932	0.7159	**0.7727**	0.5682	**0.6932**	0.7159
Brainnetome atlas	ADHD	acc	0.6613	**0.8387**	0.2258	0.8065	0.6613	0.7581	0.8065
		Sensitivity	0.6452	**0.8387**	0.3226	0.9032	0.6129	0.7419	0.7097
		Specificity	0.6774	**0.8387**	0.129	0.7097	0.7097	0.7742	0.9032
		auc	0.6613	**0.8387**	0.2258	0.8065	0.6613	0.7581	0.8065
	BP	acc	0.25	0.8235	0.5882	0.7941	0.5588	0.8529	**0.8529**
		Sensitivity	0.0294	0.7941	0.5294	0.8529	0.5	0.8529	**0.8235**
		Specificity	0.4706	0.8529	0.6471	0.7353	0.6176	0.8529	**0.8824**
		auc	0.25	0.8235	0.5882	0.7941	0.5588	0.8529	**0.8529**
	SCHZ	acc	0.5568	0.7841	0.5909	0.7955	0.0909	**0.8068**	0.8295
		Sensitivity	0.4318	0.8182	0.5909	0.8636	0.0227	**0.7727**	0.8182
		Specificity	0.6818	0.75	0.5909	0.7273	0.1591	**0.8409**	0.8409
		auc	0.5568	0.7841	0.5909	0.7955	0.0909	**0.8068**	0.8295
Power atlas	ADHD	acc	0.5968	**0.8548**	0.5323	0.7097	0.6613	0.7258	0.8065
		Sensitivity	0.8065	**0.871**	0.4516	0.9032	0.7742	0.7742	0.7742
		Specificity	0.3871	**0.8387**	0.6129	0.5161	0.5484	0.6774	0.8387
		auc	0.5968	**0.8548**	0.5323	0.7097	0.6613	0.7258	0.8065
	BP	acc	0.1176	0.75	0.4265	0.7206	0.1176	0.8088	**0.8824**
		Sensitivity	0.1176	0.7647	0.3824	0.8235	0.2353	0.7941	**0.8824**
		Specificity	0.1176	0.7353	0.4706	0.6176	0	0.8235	**0.8824**
		auc	0.1176	0.75	0.4265	0.7206	0.1176	0.8088	**0.8824**
	SCHZ	acc	0.6023	0.75	0.5909	0.75	0.0568	**0.7841**	0.7386
		Sensitivity	0.5682	0.7727	0.5227	0.8409	0.0455	**0.7955**	0.7273
		Specificity	0.6364	0.7273	0.6591	0.6591	0.0682	**0.7727**	0.75
		auc	0.6023	0.75	0.5909	0.75	0.0568	**0.7841**	0.7386

Note: Bold values represent the relative best classification result.

Santos and colleagues (dos Santos Siqueira et al., 2014) performed an ADHD classification task using functional connectivity from rs-fMRI in the ADHD-200 database. They found that brain regions in the motor network and DMN contains the most predictive information.

Besides, the functional networks affected by ADHD reported in the above studies are mainly concentrated in SMN, DMN, VN, and FPN, which is the same as the results of this experiment. Xia et al. (2014) analyzed 22 ADHD and 22 HC using a graph theory approach for the best classification accuracy and the critical brain regions. Specifically, they correlated functional brain network properties (such as topology and node pairings) with clinical SCHZ. Visual network-based analysis showed that ADHD had significantly lower local and nodal efficiencies in the frontal and occipital regions. Measures of degree centrality and between centrality showed a functional decline in the right supramarginal gyrus. At the same time, the right supramarginal gyrus showed a significant positive correlation with clinical scales in the correlation analysis. Finally, they concluded that the atypical topology of the visual network corresponds to typical ADHD

TABLE 6 The top 10 with the most prominent weight of SVM in classification

	Number	ROI	Weight
ADHD(DiffEn)	1	L_Lateral occipital cortex, superior division	0.237407
	2	R_Supramarginal gyrus, anterior division	0.206129
	3	L_Cuneal cortex	0.198669
	4	L_Occipital pole	0.186768
	5	R_Cuneal cortex	0.154033
	6	L_Postcentral gyrus	0.15394
	7	L_Cuneal cortex	0.149639
	8	R_Cingulate gyrus, posterior division	0.149421
	9	L_Inferior temporal gyrus, temporooccipital part	0.148217
	10	L_Frontal pole	0.132105
BP(SaEn)	1	L_Middle temporal gyrus, posterior division	0.425164
	2	R_Middle frontal gyrus	0.416916
	3	R_Middle temporal gyrus, posterior division	0.407243
	4	R_Frontal medial cortex	0.307743
	5	L_Frontal pole	0.301287
	6	R_Precentral gyrus	0.291573
	7	R_Temporal fusiform cortex, posterior division	0.287722
	8	R_Postcentral gyrus	0.285654
	9	L_Lateral occipital cortex, superior division	0.281492
	10	R_Lateral occipital cortex, inferior division	0.276616
SCHZ(FuEn)	1	L_Frontal pole	0.063935
	2	R_Superior temporal gyrus, posterior division	0.062686
	3	R_Angular gyrus	0.061987
	4	R_Frontal pole	0.058682
	5	L_Frontal pole	0.053862
	6	L_Frontal pole	0.053552
	7	R_Supramarginal gyrus, posterior division	0.047822
	8	R_Supramarginal gyrus, posterior division	0.046088
	9	R_Frontal orbital cortex	0.043933
	10	L_Frontal pole	0.039719

symptoms. Bollmann and colleagues (Poil et al., 2014) studied spatial working memory in adults with ADHD. They found that the left lateral occipital cortex, middle frontal gyrus, and supramarginal gyrus positively affected working memory load.

In contrast, the frontal pole, middle temporal gyrus, and occipital pole cingulate gyrus negatively affected working memory load. Tang et al. (2018) used multicenter data to analyze local and global differences between individuals with ADHD and typically developing. They found that the ALFF, the fraction ALFF, and the ReHo in the ADHD group were significantly higher in the medial orbital compared with the typically developing group. There were abnormalities in the frontal cortex, anterior cingulate cortex, postcentral gyrus, thalamus, precuneus, and cerebellum. Meanwhile, from the perspective of brain development, brain network development was delayed in the ADHD group, especially in the DMN. The cingulate gyrus is involved in attentional processing and executive function (Makris et al., 2005, 2007). Basay and colleagues (Herken et al., 2016) found that ADHD may affect white matter development in the right posterior cingulate, thereby altering the functional connectivity of white matter in the right posterior cingulate. Zhang and colleagues (Herken et al., 2016) used independent component analysis to compare the functional connectivity of 88 ADHD, and 67 typically developing subjects and found that compared with the typically developing group, the functional connectivity of the right superior occipital gyrus, left superior marginal gyrus, right superior parietal gyrus, and left middle temporal gyrus decreased. In particular, in a study (dos Santos Siqueira et al., 2014) that also used SVM linear checking to classify ADHD and typically to develop, their results found that the brain regions in the SMN, FPN, and DMN contained the most predictive information. At the same time, several cerebellar and cortical regions, including the left cerebellum, cerebellar vermis, bilateral occipital cortex, left inferior temporal gyrus, left parietal cortex, right dorsolateral prefrontal cortex, and left frontal pole also had high classification weights.

4.2.2 | BP and HC

Zhang et al. (2021) used multiscale sample entropy (MSE) of rs-fMRI computed from SCHZ, BP, and HC groups to assess differences in rs-fMRI signal complexity and found that patients (SCHZ, BP) group's MSE value decreased. SCHZ and BP showed lower complexity than HC in brain regions of the default mode, occipital, and cerebellar networks, such as precuneus, supraoccipital gyrus, and lingual gyrus cerebellum. SCHZ and BP showed higher complexity than HC in other DMN regions, such as the cingulate, thalamus, hippocampus, middle temporal gyrus, and middle frontal gyrus. From the literature (Syan et al., 2018), it can be found that, compared with controls, BP has rsFC in internal domains of the DMN such as the medial prefrontal cortex, cingulate cortex, lateral prefrontal cortex, and amygdala rsFC abnormalities. Further, rsFC changes between the amygdala, prefrontal cortex, and cingulate cortex may reflect the neural correlates of subthreshold symptoms experienced during BP remission. Moreover, the low connectivity of the DMN compared to HC may reflect the psychiatric history of patients with BP. Li et al. (2017) studied the rsFC in patients with BP and found decreased centralization of the brain region responsible for sensory processing, the lingual gyrus.

To explore the resting-state network activity of BP in remission, Bellani et al. (2020) used data from 15 BP and 27 HC subjects; within-network analysis revealed decreased connectivity in visual, motor, and cerebellar networks in patients with BP. Inter-network analysis revealed that BP increased connectivity between the motor network and the DMN, partially overlapping with the frontoparietal network. It can be seen from the above research that the differences between BP and HC are mainly concentrated in DMN, SMN, and VN, which is consistent with the results of this experiment. Zeng et al. (2020) analyzed BP and HC using cerebral blood flow perfusion imaging. They found that gray matter cerebral blood flow in BP was higher in the right lateral occipital cortex and middle temporal gyrus than in the HC lower.

Meanwhile, BP gray matter cerebral blood flow was higher in the left lateral occipital cortex, which is thought to be associated with poorer working memory, verbal memory, attention, and processing speed. In an fMRI study of adolescent BP, Gao et al. (2014) used ReHo to analyze 17 BP subjects (10–18 years) and 18 age-sex-matched HC. It was found that the ReHo values in the middle frontal gyrus, bilateral middle frontal gyrus, and middle temporal gyrus were decreased in BP compared with the control group. The correlation between the ReHo values of various brain regions and the severity of depressive symptoms in BP showed that the clinical scale in BP had a significant negative correlation with the mean ReHo values of the right middle frontal gyrus. Wang et al. (2016) analyzed 37 BP subjects and 37 HC using whole-brain functional connectivity. The results showed that compared with the HC group, the BD group had a higher DMN (i.e., bilateral medial prefrontal cortex, bilateral middle temporal gyrus, left precuneus, and right posterior cingulate cortex), and right supramarginal gyrus. The functional connectivity strength of the angular gyrus decreased, and the functional connectivity strength increased in the bilateral temporal poles. Achalia et al. (2019) used ReHo to analyze spontaneous brain activity in 20 BP subjects and 20 age-, sex-, and education-matched HC; results illustrate that compared with the HC, ReHo in the BP group was significantly increased in the right precuneus, right insula, right supramarginal gyrus, and right precentral gyrus. Meanwhile, compared with the HC, the ReHo value of the BP group was not significantly decreased.

4.2.3 | SCHZ and HC

Yu et al. (2013) explored patterns of rs-fMRI in SCHZ and their healthy siblings. The results showed changes in rsFC in regions within the DMN and the cerebellar network, such as the hippocampus, medial prefrontal cortex, middle temporal gyrus, parietal gyrus, and some cerebellar regions. Moreover, FCs between the cerebellum and the prefrontal, middle temporal gyrus, thalamus, and middle temporal pole showed high discrimination. A treatment-resistant SCHZ (Yentes et al., 2012) found decreased fALFF in the medial prefrontal and orbitofrontal cortices and DMNs in bilateral putamen with increased rsFC in the left insula and bilateral dorsal prefrontal cortex. In SCHZ, ALFF was reduced in the bilateral ventral frontal cortex (Lui et al., 2010). SCHZ exhibits high connectivity between subcortical and auditory networks (Lottman et al., 2019). It can be seen from the above studies that the difference between SCHZ and HC is mainly concentrated in DMN.

Meanwhile, this experiment also found significant differences in SMN and VN. SCHZ is associated with dysfunction in visual perception, and the right lateral occipital cortex is a mid-level visual area critical for object recognition. Previous fMRI studies have reported structural and functional abnormalities in the lateral occipital cortex of SCHZ (Cant & Goodale, 2007). Li et al. (2020) investigated the spatiotemporal interactions of the lateral occipital cortex with other brain networks through functional connectivity. They found that the temporal instability of lateral occipital cortical connections was increased in both resting-state and task-switching situations, and in the resting state, compared to controls, the patients' lateral occipital cortex interacted with the FPN and thalamus effect increased. At the same time, the interaction of the lateral occipital cortex with the DMN increased during task switching. The study also found that temporal instability of lateral occipital cortical connectivity was positively associated with patients' switching costs during task performance and the severity of hallucinations. These results suggest that reduced stability of lateral occipital cortical connections may be an important factor in neurocognitive dysfunction and symptom severity in SCHZ. The thalamus regulates input from multiple brain regions, is considered a major relay hub, and may play a specific role in SCHZ pathophysiology (Shenton et al., 2001). Gifford and colleagues (Gifford et al., 2020) compared flexibility in 55 SCHZ and 72 HC. The study found that nodes covering the left thalamus had significantly higher flexibility scores at the node level.

The temporal plane, located posterior to the superior temporal lobe, is a vital brain area associated with language and speech production (Galaburda, 1978) and is also thought to be involved in the pathophysiology of SCHZ (Shenton et al., 1992). Kwon et al. (1999) used

magnetic resonance imaging to measure subtemporal gray matter in 16 SCHZ, and 16 HC matched for age, sex, handedness, and parental economic status volume. The study found that gray matter volume in the left temporal plane was significantly reduced (28.2%) in the SCHZ group compared to the HC group. The left temporal plane was more asymmetric than the right temporal plane in the SCHZ group in the HC group. Found the opposite result, which is thought to be the basis of language processing impairment and SCHZ-specific paranoia. Zhou et al. (2010) analyzed the functional connectivity of 19 early-stage SCHZ and 19 HC and found that the functional connectivity strength increased in the left inferior temporal gyrus. An fMRI study using meta-analysis (Taylor et al., 2012) found that the HC showed stronger activation in the left occipital pole than the SCHZ group in terms of affective experience.

5 | CONCLUSIONS

This article will thoroughly discuss the differences between ADHD, BP, and SCHZ (31 healthy control and 31 ADHD; 34 healthy control and 34 BP; 42 healthy control and 42 SCHZ) relative to healthy subjects in combination with three atlases (et al., the Brainnetome atlas, the Dosenbach atlas, Power atlas) and seven entropies (et al., ApEn, SaEn, PeEn, FuEn, DiffEn, RaEn, and DispEn). We found a difference between HC and ADHD, BP, and SCHZ, specifically, cingulo-opercular > (occipital DMN and frontoparietal) in ADHD, cingulo-opercular > (occipital, DMN, and frontoparietal) in BP, (cingulo-opercular, DMN, and occipital) > frontoparietal in SCHZ. Regardless of the atlas used, the mean multiscale entropy values for the ADHD, BP, and SCHZ were significantly lower than for the HCs. Furthermore, the performance of different multiscale entropy algorithms on different diseases is also different, such as DiffEn, RaEn, and SaEn performed better in ADHD, SCHZ, and BP, respectively. The ADHD classification results show that DiffEn performs the best, where DiffEn achieves an accuracy of 0.8548. Among the classification results of BP, SaEn performs the best, where SaEn achieves an accuracy of 0.8824. For the classification results of SCHZ, RaEn performs the best, where RaEn achieves an accuracy of 0.8409. Besides, the top 10 key brain regions of the weight ranking of entropy corresponding to SVM of each disease were also obtained.

5.1 | Limitations

Although this article considers the performance of seven different entropies on ADHD, BP, and SCHZ and then extends these to multiscale and three different atlases, this article's amount of rs-fMRI data is not large enough, which is also the main disadvantage. The next project will explore this topic by collecting multiple sites' rs-fMRI data. Besides, three parameters (N is the number of time points, m specifies the dimension of the phase space, and r is the similarity tolerance) selection for each entropy method is limited. Although already some journals have discussed the setting of these parameters (Azami & Escudero, 2018; Bandt & Pompe, 2002; Li et al., 2014; Schultz et al., 2008; Tocado et al., 2009), how to get a more suitable parameter was still not sure. So, based on our previous works (Guan et al., 2020, 2022), the nonlinear complexity of rs-fMRI will further explore the more suitable parameters.

ACKNOWLEDGMENTS

This work was supported by the National Natural Science Foundation of China (61871420), the Central Universities Foundation, Southwest Minzu University (2021XJTD01), the introduction of talent, Southwest MinZu University, funding research projects start (RQD2021064), and the Natural Science Foundation of Henan Polytechnic University (B2021-38).

DATA AVAILABILITY STATEMENT

The MSC dataset is publicly available at https://openneuro.org/datasets/ds000224, and the UCLA dataset is publicly available at the OpenfMRI database with the accession number ds000030 (https://www.openfmri.org/dataset/ds000030/). Data were processed using publicly available software (SPM12 http://www.fil.ion.ucl.ac.uk/spm/software/spm12/ and DPAPI http://rfmri.org/DPABI). The simulation time-series and seven entropy methods were performed using MATLAB code available from the authors upon request.

ORCID

Chun Meng https://orcid.org/0000-0003-0145-6627

Bharat B. Biswal https://orcid.org/0000-0002-3710-3500

REFERENCES

Achalia, R., Jacob, A., Achalia, G., Sable, A., Venkatasubramanian, G., & Rao, N. (2019). Investigating spontaneous brain activity in bipolar disorder: A resting-state functional magnetic resonance imaging study. *Indian Journal of Psychiatry*, *61*(6), 630–634. https://doi.org/10.4103/psychiatry.IndianJPsychiatry_391_19

Akdeniz, G. (2017). Complexity analysis of resting-state fMRI in adult patients with attention deficit hyperactivity disorder: Brain entropy. *Computational Intelligence and Neuroscience*, *2017*, 1–6. https://doi.org/10.1155/2017/3091815

Ali, Z., Hossain, M. S., Muhammad, G., & Aslam, M. (2018). New zero-watermarking algorithm using Hurst exponent for protection of privacy in telemedicine. *IEEE Access*, *6*, 7930–7940. https://doi.org/10.1109/access.2018.2799604

Ashburner, J. (2012). SPM: A history. *NeuroImage*, *62*(2), 791–800. https://doi.org/10.1016/j.neuroimage.2011.10.025

Azami, H., & Escudero, J. (2018). Amplitude- and fluctuation-based dispersion entropy. *Entropy*, *20*(3), 210. https://doi.org/10.3390/e20030210

Bandt, C., & Pompe, B. (2002). Permutation entropy: A natural complexity measure for time series. *Physical Review Letters*, *88*(17), 174102. https://doi.org/10.1103/PhysRevLett.88.174102

Bellani, M., Bontempi, P., Zovetti, N., Gloria Rossetti, M., Perlini, C., Dusi, N., Squarcina, L., Marinelli, V., Zoccatelli, G., Alessandrini, F., Francesca Maria Ciceri, E., Sbarbati, A., & Brambilla, P. (2020). Resting state networks activity in euthymic bipolar disorder. *Bipolar Disorders*, *22*(6), 593–601. https://doi.org/10.1111/bdi.12900

Biswal, B., Yetkin, F. Z., Haughton, V. M., & Hyde, J. S. (1995). Functional connectivity in the motor cortex of resting human brain using echo-planar MRI. *Magnetic Resonance in Medicine*, *34*(4), 537–541. https://doi.org/10.1002/mrm.1910340409

Biswal, B. B., Mennes, M., Zuo, X. N., Gohel, S., Kelly, C., Smith, S. M., Beckmann, C. F., Adelstein, J. S., Buckner, R. L., Colcombe, S., Dogonowski, A. M., Ernst, M., Fair, D., Hampson, M., Hoptman, M. J., Hyde, J. S., Kiviniemi, V. J., Kötter, R., Li, S. J., … Milham, M. P. (2010). Toward discovery science of human brain function. *Proceedings of the National Academy of Sciences of the United States of America*, *107*(10), 4734–4739. https://doi.org/10.1073/pnas.0911855107

Cant, J. S., & Goodale, M. A. (2007). Attention to form or surface properties modulates different regions of human Occipitotemporal cortex. *Cerebral Cortex*, *17*(3), 713–731. https://doi.org/10.1093/cercor/bhk022

Chambers, W. J. (1985). The assessment of affective disorders in children and adolescents by Semistructured interview. *Archives of General Psychiatry*, *42*(7), 696. https://doi.org/10.1001/archpsyc.1985.01790300064008

Chen, W., Wang, Z., Xie, H., & Yu, W. (2007). Characterization of surface EMG signal based on fuzzy entropy. *IEEE Transactions on Neural Systems and Rehabilitation Engineering*, *15*(2), 266–272. https://doi.org/10.1109/tnsre.2007.897025

Cortes, C., & Vapnik, V. (1995). Support-vector networks. *Machine Learning*, *20*(3), 273–297. https://doi.org/10.1023/a:1022627411411

Cortese, S., Kelly, C., Chabernaud, C., Proal, E., Di Martino, A., Milham, M. P., & Castellanos, F. X. (2012). Toward systems neuroscience of ADHD: A meta-analysis of 55 fMRI studies. *American Journal of Psychiatry*, *169*(10), 1038–1055. https://doi.org/10.1176/appi.ajp.2012.11101521

Costa, M., Goldberger, A. L., & Peng, C. K. (2005). Multiscale entropy analysis of biological signals. *Physical Review E*, *71*(2), 021906. https://doi.org/10.1103/PhysRevE.71.021906

Csermely, P., Xia, M., Wang, J., & He, Y. (2013). BrainNet viewer: A network visualization tool for human brain Connectomics. *PLoS One*, *8*(7), e68910. https://doi.org/10.1371/journal.pone.0068910

Deco, G., Jirsa, V. K., & McIntosh, A. R. (2011). Emerging concepts for the dynamical organization of resting-state activity in the brain. *Nature Reviews. Neuroscience*, *12*(1), 43–56. https://doi.org/10.1038/nrn2961

dos Santos Siqueira, A., Biazoli Junior, C. E., Comfort, W. E., Rohde, L. A., & Sato, J. R. (2014). Abnormal functional resting-state networks in ADHD: Graph theory and pattern recognition analysis of fMRI data. *BioMed Research International*, *2014*, 1–10. https://doi.org/10.1155/2014/380531

Dosenbach, N. U. F., Nardos, B., Cohen, A. L., Fair, D. A., Power, J. D., Church, J. A., Nelson, S. M., Wig, G. S., Vogel, A. C., Lessov-Schlaggar, C. N., Barnes, K. A., Dubis, J. W., Feczko, E., Coalson, R. S., Pruett, J. R., Jr., Barch, D. M., Petersen, S. E., & Schlaggar, B. L. (2010). Prediction of individual brain maturity using fMRI. *Science*, *329*(5997), 1358–1361. https://doi.org/10.1126/science.1194144

Duan, R.-N., Zhu, J.-Y., and Lu, B.-L. (2013). Differential entropy feature for EEG-based emotion classification. In *Proceedings of the 2013 6th International IEEE/EMBS Conference on Neural Engineering (NER)*.

Fan, L., Li, H., Zhuo, J., Zhang, Y., Wang, J., Chen, L., Yang, Z., Chu, C., Xie, S., Laird, A. R., Fox, P. T., Eickhoff, S. B., Yu, C., & Jiang, T. (2016). The human Brainnetome atlas: A new brain atlas based on connectional architecture. *Cerebral Cortex*, *26*(8), 3508–3526. https://doi.org/10.1093/cercor/bhw157

Ferraz, M. S. A., & Kihara, A. H. (2022). Beyond randomness: Evaluating measures of information entropy in binary series. *Physical Review E*, *105*(4), 044101. https://doi.org/10.1103/PhysRevE.105.044101

Finn, E. S., Shen, X., Scheinost, D., Rosenberg, M. D., Huang, J., Chun, M. M., Papademetris, X., & Constable, R. T. (2015). Functional connectome fingerprinting: Identifying individuals using patterns of brain connectivity. *Nature Neuroscience*, *18*(11), 1664–1671. https://doi.org/10.1038/nn.4135

Fox, M. D., & Greicius, M. (2010). Clinical applications of resting state functional connectivity. *Frontiers in Systems Neuroscience*, *4*, 19. https://doi.org/10.3389/fnsys.2010.00019

Fox, M. D., & Raichle, M. E. (2007). Spontaneous fluctuations in brain activity observed with functional magnetic resonance imaging. *Nature Reviews Neuroscience*, *8*(9), 700–711. https://doi.org/10.1038/nrn2201

Friston, K. J., Holmes, A., Poline, J. B., Price, C. J., & Frith, C. D. (1996). Detecting activations in PET and fMRI: Levels of inference and power. *NeuroImage*, *4*(3), 223–235. https://doi.org/10.1006/nimg.1996.0074

Galaburda, A. M. (1978). Human Brain. *Archives of Neurology*, *35*(12), 812. https://doi.org/10.1001/archneur.1978.00500360036007

Gao, W., Jiao, Q., Lu, S., Zhong, Y., Qi, R., Lu, D., Xiao, Q., Yang, F., Lu, G., & Su, L. (2014). Alterations of regional homogeneity in pediatric bipolar depression: A resting-state fMRI study. *BMC Psychiatry*, *14*(1), 222. https://doi.org/10.1186/s12888-014-0222-y

Gifford, G., Crossley, N., Kempton, M. J., Morgan, S., Dazzan, P., Young, J., & McGuire, P. (2020). Resting state fMRI based multilayer network configuration in patients with schizophrenia. *NeuroImage: Clinical*, *25*, 102169. https://doi.org/10.1016/j.nicl.2020.102169

Gordon, E. M., Laumann, T. O., Gilmore, A. W., Newbold, D. J., Greene, D. J., Berg, J. J., Ortega, M., Hoyt-Drazen, C., Gratton, C., Sun, H., Hampton, J. M., Coalson, R. S., Nguyen, A. L., McDermott, K. B., Shimony, J. S., Snyder, A. Z., Schlaggar, B. L., Petersen, S. E., Nelson, S. M., & Dosenbach, N. U. F. (2017). Precision functional mapping of individual human brains. *Neuron*, *95*(4), 791-+. https://doi.org/10.1016/j.neuron.2017.07.011

Greicius, M. D., Krasnow, B., Reiss, A. L., & Menon, V. (2003). Functional connectivity in the resting brain: A network analysis of the default mode hypothesis. *Proceedings of the National Academy of Sciences of the United States of America*, *100*(1), 253–258. https://doi.org/10.1073/pnas.0135058100

Greicius, M. D., Supekar, K., Menon, V., & Dougherty, R. F. (2009). Resting-state functional connectivity reflects structural connectivity in the default mode network. *Cerebral Cortex*, *19*(1), 72–78. https://doi.org/10.1093/cercor/bhn059

Guan, S., Jiang, R., Bian, H., Yuan, J., Xu, P., Meng, C., & Biswal, B. (2020). The profiles of non-stationarity and non-linearity in the time series of resting-state brain networks. *Frontiers in Neuroscience*, *14*, 493. https://doi.org/10.3389/fnins.2020.00493

Guan, S., Wan, D., Yang, Y., & Biswal, B. (2022). Sources of multifractality of the brain rs-fMRI signal. *Chaos, Solitons & Fractals*, *160*, 112222. https://doi.org/10.1016/j.chaos.2022.112222

Herken, H., Kabukçu Başay, B., Büber, A., Başay, Ö., Alacam, H., Öztürk, Ö., Suren, S., Izci Ay, O., Agladioglu, K., Erdal, M. E., Ercan, E., & Acikel, C. (2016). White matter alterations related to attention-deficit hyperactivity disorder and COMT val158met polymorphism: Children with valine homozygote attention-deficit hyperactivity disorder have altered white matter connectivity in the right cingulum (cingulate gyrus). *Neuropsychiatric Disease and Treatment*, *12*, 969–981. https://doi.org/10.2147/ndt.S104450

Ju, R., Hu, C., Zhou, P., & Li, Q. (2019). Early diagnosis of Alzheimer's disease based on resting-state brain networks and deep learning. *IEEE/ACM Transactions on Computational Biology and Bioinformatics*, *16*(1), 244–257. https://doi.org/10.1109/tcbb.2017.2776910

Kwon, J. S., McCarley, R. W., Hirayasu, Y., Anderson, J. E., Fischer, I. A., Kikinis, R., Jolesz, F. A., & Shenton, M. E. (1999). Left Planum Temporale volume reduction in schizophrenia. *Archives of General Psychiatry*, *56*(2), 142–148. https://doi.org/10.1001/archpsyc.56.2.142

Li, J., Yan, J., Liu, X., & Ouyang, G. (2014). Using permutation entropy to measure the changes in EEG signals during absence seizures. *Entropy*, *16*(6), 3049–3061. https://doi.org/10.3390/e16063049

Li, K., Sweeney, J. A., & Hu, X. P. (2020). Context-dependent dynamic functional connectivity alteration of lateral occipital cortex in schizophrenia. *Schizophrenia Research*, *220*, 201–209. https://doi.org/10.1016/j.schres.2020.03.020

Li, M., Das, T., Deng, W., Wang, Q., Li, Y., Zhao, L., Ma, X., Wang, Y., Yu, H., Li, X., Meng, Y., Palaniyappan, L., & Li, T. (2017). Clinical utility

of a short resting-state MRI scan in differentiating bipolar from unipolar depression. *Acta Psychiatrica Scandinavica*, *136*(3), 288–299. https://doi.org/10.1111/acps.12752

Lin, C., Lee, S.-H., Huang, C.-M., Chen, G.-Y., Ho, P.-S., Liu, H.-L., Chen, Y. L., Lee, T. M. C., & Wu, S. C. (2019). Increased brain entropy of resting-state fMRI mediates the relationship between depression severity and mental health-related quality of life in late-life depressed elderly. *Journal of Affective Disorders*, *250*, 270–277. https://doi.org/10.1016/j.jad.2019.03.012

Lin, L., Chang, D., Song, D., Li, Y., & Wang, Z. (2022). Lower resting brain entropy is associated with stronger task activation and deactivation. *NeuroImage*, *249*, 118875. https://doi.org/10.1016/j.neuroimage.2022.118875

Liu, M., Liu, X., Hildebrandt, A., & Zhou, C. (2020). Individual cortical entropy profile: Test–retest reliability, predictive power for cognitive ability, and neuroanatomical foundation. *Cerebral Cortex Communications*, *1*(1), tgaa015. https://doi.org/10.1093/texcom/tgaa015

Lottman, K. K., Gawne, T. J., Kraguljac, N. V., Killen, J. F., Reid, M. A., & Lahti, A. C. (2019). Examining resting-state functional connectivity in first-episode schizophrenia with 7T fMRI and MEG. *NeuroImage: Clinical*, *24*, 101959. https://doi.org/10.1016/j.nicl.2019.101959

Lui, S., Li, T., Deng, W., Jiang, L., Wu, Q., Tang, H., Yue, Q., Huang, X., Chan, R. C., Collier, D. A., Meda, S. A., Pearlson, G., Mechelli, A., Sweeney, J. A., & Gong, Q. (2010). Short-term effects of antipsychotic treatment on cerebral function in drug-naive first-episode schizophrenia revealed by "resting state" functional magnetic resonance imaging. *Archives of General Psychiatry*, *67*(8), 783–792. https://doi.org/10.1001/archgenpsychiatry.2010.84

Makris, N., Buka, S. L., Biederman, J., Papadimitriou, G. M., Hodge, S. M., Valera, E. M., Brown, A. B., Bush, G., Monuteaux, M. C., Caviness, V. S., Kennedy, D. N., & Seidman, L. J. (2007). Attention and executive systems abnormalities in adults with childhood ADHD: A DT-MRI study of connections. *Cerebral Cortex*, *18*(5), 1210–1220. https://doi.org/10.1093/cercor/bhm156

Makris, N., Kennedy, D. N., McInerney, S., Sorensen, A. G., Wang, R., Caviness, V. S., et al. (2005). Segmentation of subcomponents within the superior longitudinal fascicle in humans: A quantitative, In vivo, DT-MRI study. *Cerebral Cortex*, *15*(6), 854–869. https://doi.org/10.1093/cercor/bhh186

Marinazzo, D., Kosciessa, J. Q., Kloosterman, N. A., & Garrett, D. D. (2020). Standard multiscale entropy reflects neural dynamics at mismatched temporal scales: What's signal irregularity got to do with it? *PLoS Computational Biology*, *16*(5), e1007885. https://doi.org/10.1371/journal.pcbi.1007885

Niu, Y., Cao, R., Wang, H., Li, C., Zhou, M., Guo, Y., Wang, B., Yan, P., & Xiang, J. (2019). Permutation fuzzy entropy—An index for the analysis of epileptic electroencephalogram. *Journal of Medical Imaging and Health Informatics*, *9*(3), 637–645. https://doi.org/10.1166/jmihi.2019.2584

Niu, Y., Sun, J., Wang, B., Hussain, W., Fan, C., Cao, R., Zhou, M., & Xiang, J. (2020). Comparing test-retest reliability of entropy methods: Complexity analysis of resting-state fMRI. *IEEE Access*, *8*, 124437–124450. https://doi.org/10.1109/access.2020.3005906

Omidvarnia, A., Mesbah, M., Pedersen, M., & Jackson, G. (2018). Range entropy: A bridge between signal complexity and self-similarity. *Entropy*, *20*(12), 962. https://doi.org/10.3390/e20120962

Poil, S. S., Bollmann, S., Ghisleni, C., O'Gorman, R. L., Klaver, P., Ball, J., Eich-Höchli, D., Brandeis, D., & Michels, L. (2014). Age dependent electroencephalographic changes in attention-deficit/hyperactivity disorder (ADHD). *Clinical Neurophysiology*, *125*(8), 1626–1638. https://doi.org/10.1016/j.clinph.2013.12.118

Poldrack, R. A., Congdon, E., Triplett, W., Gorgolewski, K. J., Karlsgodt, K. H., Mumford, J. A., Sabb, F. W., Freimer, N. B., London, E. D., Cannon, T. D., & Bilder, R. M. (2016). A phenome-wide examination of neural and cognitive function. *Scientific Data*, *3*(1), 160110. https://doi.org/10.1038/sdata.2016.110

Power, J. D., Cohen, A. L., Nelson, S. M., Wig, G. S., Barnes, K. A., Church, J. A., Vogel, A. C., Laumann, T. O., Miezin, F. M., Schlaggar, B. L., & Petersen, S. E. (2011). Functional network organization of the human brain. *Neuron*, *72*(4), 665–678.

Richman, J. S., Lake, D. E., & Moorman, J. R. (2004). Sample entropy. *Methods in Enzymology*, *384*, 172–184.

Richman, J. S., & Moorman, J. R. (2000). Physiological time-series analysis using approximate entropy and sample entropy. *American Journal of Physiology. Heart and Circulatory Physiology*, *278*(6), H2039–H2049. https://doi.org/10.1152/ajpheart.2000.278.6.H2039

Rongsawad, K., Worawan, L., Jirarojprapa, K., Kaewkham, S., & Khattiwong, S. (2019). 72 test-retest reliability and minimal detectable change for postural sway by using sway meter in elderly subjects. *Age and Ageing*, *48*(Supplement_4), iv18–iv27. https://doi.org/10.1093/ageing/afz164.72

Rostaghi, M., & Azami, H. (2016). Dispersion entropy: A measure for time-series analysis. *IEEE Signal Processing Letters*, *23*(5), 610–614. https://doi.org/10.1109/lsp.2016.2542881

Schultz, A., Siedenberg, M., Grouven, U., Kneif, T., & Schultz, B. (2008). Comparison of Narcotrend index, Bispectral index, spectral and entropy parameters during induction of propofol-remifentanil anaesthesia. *Journal of Clinical Monitoring and Computing*, *22*(2), 103–111. https://doi.org/10.1007/s10877-008-9111-6

Shenton, M. E., Dickey, C. C., Frumin, M., & McCarley, R. W. (2001). A review of MRI findings in schizophrenia. *Schizophrenia Research*, *49*(1–2), 1–52. https://doi.org/10.1016/s0920-9964(01)00163-3

Shenton, M. E., Kikinis, R., Jolesz, F. A., Pollak, S. D., LeMay, M., Wible, C. G., Hokama, H., Martin, J., Metcalf, D., Coleman, M., & McCarley, R. W. (1992). Abnormalities of the left temporal lobe and thought disorder in schizophrenia. *New England Journal of Medicine*, *327*(9), 604–612. https://doi.org/10.1056/nejm199208273270905

Shrout, P. E., & Fleiss, J. L. (1979). Intraclass correlations: Uses in assessing rater reliability. *Psychological Bulletin*, *86*(2), 420–428. https://doi.org/10.1037//0033-2909.86.2.420

Smith, R. X., Yan, L., & Wang, D. J. J. (2013). Multiple time scale complexity analysis of resting state FMRI. *Brain Imaging and Behavior*, *8*(2), 284–291. https://doi.org/10.1007/s11682-013-9276-6

Sokunbi, M., Gradin, V. B., Waiter, G. D., Cameron, G. G., Ahearn, T. S., Murray, A. D., Steele, D. J., & The PLoS One Staff. (2014). Nonlinear complexity analysis of brain FMRI signals in schizophrenia. *PLoS One*, *9*(5), e95146. https://doi.org/10.1371/journal.pone.0095146

Sokunbi, M. A. S., Staff, R. T., Waiter, G. D., Cameron, G. G., Ahearn, T. S., & Murray, A. (2011). Functional MRI entropy measurements of age-related brain changes. In *Proceedings of the 17th Annual Meeting of the Organization for Human Brain Mapping*, Quebec City, Canada.

Sokunbi, M. O., Cameron, G. G., Ahearn, T. S., Murray, A. D., & Staff, R. T. (2015). Fuzzy approximate entropy analysis of resting state fMRI signal complexity across the adult life span. *Medical Engineering & Physics*, *37*(11), 1082–1090. https://doi.org/10.1016/j.medengphy.2015.09.001

Sokunbi, M. O., Fung, W., Sawlani, V., Choppin, S., Linden, D. E. J., & Thome, J. (2013). Resting state fMRI entropy probes complexity of brain activity in adults with ADHD. *Psychiatry Research: Neuroimaging*, *214*(3), 341–348. https://doi.org/10.1016/j.pscychresns.2013.10.001

Spitzer, R. L. (1992). The structured clinical interview for DSM-III-R (SCID). *Archives of General Psychiatry*, *49*(8), 624. https://doi.org/10.1001/archpsyc.1992.01820080032005

Sun, Y., Zhao, L., Lan, Z., Jia, X.-Z., & Xue, S.-W. (2020). Differentiating boys with ADHD from those with typical development based on whole-brain functional connections using a machine learning approach. *Neuropsychiatric Disease and Treatment*, *16*, 691–702. https://doi.org/10.2147/ndt.S239013

Sutcubasi, B., Metin, B., Kurban, M. K., Metin, Z. E., Beser, B., & Sonuga-Barke, E. (2020). Resting-state network dysconnectivity in ADHD: A system-neuroscience-based meta-analysis. *The World Journal of Biological Psychiatry*, *21*(9), 662–672. https://doi.org/10.1080/15622975.2020.1775889

Syan, S. K., Smith, M., Frey, B. N., Remtulla, R., Kapczinski, F., Hall, G. B. C., & Minuzzi, L. (2018). Resting-state functional connectivity in individuals with bipolar disorder during clinical remission: A systematic review. *Journal of Psychiatry & Neuroscience*, *43*(5), 298–316. https://doi.org/10.1503/jpn.170175

Tang, C., Wei, Y., Zhao, J., & Nie, J. (2018). Different developmental pattern of brain activities in ADHD: A study of resting-state fMRI. *Developmental Neuroscience*, *40*(3), 246–257. https://doi.org/10.1159/000490289

Taylor, S. F., Kang, J., Brege, I. S., Tso, I. F., Hosanagar, A., & Johnson, T. D. (2012). Meta-analysis of functional neuroimaging studies of emotion perception and experience in schizophrenia. *Biological Psychiatry*, *71*(2), 136–145. https://doi.org/10.1016/j.biopsych.2011.09.007

Tocado, L., Palacios, E., & Burriel, R. (2009). Entropy determinations and magnetocaloric parameters in systems with first-order transitions: Study of MnAs. *Journal of Applied Physics*, *105*(9), 093918. https://doi.org/10.1063/1.3093880

Van Essen, D. C., Smith, S. M., Barch, D. M., Behrens, T. E. J., Yacoub, E., & Ugurbil, K. (2013). The WU-Minn human connectome project: An overview. *NeuroImage*, *80*, 62–79. https://doi.org/10.1016/j.neuroimage.2013.05.041

Wang, Y., Zhong, S., Jia, Y., Sun, Y., Wang, B., Liu, T., Pan, J., & Huang, L. (2016). Disrupted resting-state functional connectivity in nonmedicated bipolar disorder. *Radiology*, *280*(2), 529–536. https://doi.org/10.1148/radiol.2016151641

Xia, S., Foxe, J. J., Sroubek, A. E., Branch, C., & Li, X. (2014). Topological organization of the "small-world" visual attention network in children with attention deficit/hyperactivity disorder (ADHD). *Frontiers in Human Neuroscience*, *8*, 162. https://doi.org/10.3389/fnhum.2014.00162

Yakovleva, T. V., Kutepov, I. E., Karas, A. Y., Yakovlev, N. M., Dobriyan, V. V., Papkova, I. V., Zhigalov, M. V., Saltykova, O. A., Krysko, A. V., Yaroshenko, T. Y., Erofeev, N. P., & Krysko, V. A. (2020). EEG analysis in structural focal epilepsy using the methods of nonlinear dynamics (Lyapunov exponents, Lempel–Ziv complexity, and multiscale entropy). *The Scientific World Journal*, *2020*, 1–13. https://doi.org/10.1155/2020/8407872

Yan, C. G., Wang, X. D., Zuo, X. N., & Zang, Y. F. (2016). DPABI: Data Processing & Analysis for (resting-state) brain imaging. *Neuroinformatics*, *14*(3), 339–351. https://doi.org/10.1007/s12021-016-9299-4

Yentes, J. M., Hunt, N., Schmid, K. K., Kaipust, J. P., McGrath, D., & Stergiou, N. (2012). The appropriate use of approximate entropy and sample entropy with short data sets. *Annals of Biomedical Engineering*, *41*(2), 349–365. https://doi.org/10.1007/s10439-012-0668-3

Yu, Y., Shen, H., Zhang, H., Zeng, L.-L., Xue, Z., & Hu, D. (2013). Functional connectivity-based signatures of schizophrenia revealed by multiclass pattern analysis of resting-state fMRI from schizophrenic patients and their healthy siblings. *Biomedical Engineering Online*, *12*(1), 1–13. https://doi.org/10.1186/1475-925x-12-10

Zeng, V., Lizano, P., Bolo, N. R., Lutz, O., Brady, R., Ivleva, E. I., et al. (2020). Altered cerebral perfusion in bipolar disorder: A pCASL MRI study. *Bipolar Disorders*, *23*(2), 130–140. https://doi.org/10.1111/bdi.12966

Zhang, N., Niu, Y., Sun, J., An, W., Li, D., Wei, J., Yan, T., Xiang, J., & Wang, B. (2021). Altered complexity of spontaneous brain activity in schizophrenia and bipolar disorder patients. *Journal of Magnetic Resonance Imaging*, *54*, 586–595. https://doi.org/10.1002/jmri.27541

Zhou, B., Tan, C., Tang, J., & Chen, X. (2010). Brain functional connectivity of functional magnetic resonance imaging of patients with early-onset schizophrenia. *Journal of Central South University. Medical Sciences*, *35*(1), 17–24. https://doi.org/10.3969/j.issn.1672-7347.2010.01.003

How to cite this article: Guan, S., Wan, D., Zhao, R., Canario, E., Meng, C., & Biswal, B. B. (2023). The complexity of spontaneous brain activity changes in schizophrenia, bipolar disorder, and ADHD was examined using different variations of entropy. *Human Brain Mapping*, *44*(1), 94–118. https://doi.org/10.1002/hbm.26129